Penerbit Akademia Baru

CFD Letters

Journal homepage: www.akademiabaru.com/cfdl.html
ISSN: 2180-1363

Heat and Mass Transfer of A MHD Flow of a Nanofluid Through a Porous Medium in an Annular, Circular Region with Outer Cylinder Maintained at Constant Heat Flux

Open

Madduleti Nagasasikala[1], Bommanna Lavanya[2,*]

[1] Department of Mathematics, Govt. Degree College (Autonomous), Anantapuramu-515001, A.P, India
[2] Department of Mathematics Assistant Professor senior Grade MIT MAHE, Manipal-576104, KA, India

ARTICLE INFO

Article history:
Received 4 May 2019
Received in revised form 7 August 2019
Accepted 12 September 2019
Available online 29 September 2019

Keywords:
Shear stress; Heat transfer; Mass transfer; convection

ABSTRACT

In this paper we consider the unsteady thermal convection due to the imposed traveling thermal wave boundary through a vertical channel bounded by flat walls. Before in few papers have discussed the two dimensional free and forced convection flow and heat transfer in a vertical wavy channel with traveling thermal waves embedded in a porous medium but here we are considering The effect of free convective heat and mass transfer flow have been discussed by solving the governing unsteady non-linear equations under perturbation scheme. The velocity, the temperature and the concentration have been analyzed for different variations of the governing parameters. The shear stress, rate of heat transfer and rate of mass transfer have been evaluated and tabulated for these sets of parameters and also from tables we analyze rate of heat and mass transfer for different parametric values.

1. Introduction

There are many transport processes in nature and in many industries where flows with free convection currents caused by the temperature differences are affected by the differences in concentration or material constitutions. In a number of engineering applications foreign gases are injected to attain more efficiency, the advantage being the reduction in wall shear stress, the mass transfer conductance or the rate of heat transfer. Gases such as H_2, H_2O, CO_2, etc., are usually used as foreign gases in air flowing past bodies. So the problems of heat and mass transfer past vertical bodies in boundary layer flows have been studied by many of whom the names of Somers [1], Gil *et al*. [2], Adeams and Lowell [3] and Gebhart and Peera [4] are worth mentioning. Lavanya [5] studied Unsteady MHD Convective laminar flow between two Vertical Porous plates with mass transfer.

The combined effects of thermal and mass diffusion in channel flows has been studied in the recent times by a few authors notably. Nelson and wood [6, 7] have presented numerical analysis of developing laminar flow between vertical parallel plates for combined heat and mass transfer natural

* *Corresponding author.*
E-mail address: lavanya.b@manipal.edu (Bommanna Lavanya)

convection with uniform wall temperature and concentration boundary conditions. Lavanya [8, 9] studied Effects of Dissipation and Radiation on Heat Transfer Flow of a Convective Rotating Cuo-Water Nano-fluid in a Vertical Channel and MHD Rotating flow through a porous medium with Heat and mass transfer.

Vajravelu and Debnath [10] have made an interesting and a detailed study of non-linear convection heat transfer and fluid flows, induced by traveling thermal waves. Lavanya [11, 12] have studied the radiation and chemical reaction effects on MHD flow over an infinite vertical oscillating porous plate with soret effect and the author also studied radiation and mass transfer effects on MHD marangoni convection over a flat surface in presence of joule heating, viscous dissipation, heat generation with suction and injection. Guria and Jana [13] have discussed the two dimensional free and forced convection flow and heat transfer in a vertical wavy channel with traveling thermal waves embedded in a porous medium. The set of non-linear ordinary differential equations are solved analytically. The velocity and temperature fields have been obtained using perturbation technique. Ny *et al*. [14] studied Numerical Study on Turbulent-Forced Convective Heat Transfer of Ag/Heg Water Nanofluid in Pipe. Dero *et al.* [15] studied MHD micropolar nanofluid flow over an exponentially stretching/shrinking surface. H.A. Mohammed, et.al studied Mixed Convective Nanofluids Flow in a Channel having Forward-Facing Step with Baffle Lavanya *et al.* [17] studied the effect of radiation on free convection heat and mass transfer flow through porous medium in a vertical channel with heat absorption/generation and chemical reaction.

In this paper we consider the unsteady thermal convection due to the imposed traveling thermal wave boundary through a vertical channel bounded by flat walls. The effect of free convective heat and mass transfer flow have been discussed by solving the governing unsteady non-linear equations under perturbation scheme. The velocity, the temperature and the concentration have been analyzed for different variations of the governing parameters. The shear stress, rate of heat transfer and rate of mass transfer have been evaluated and tabulated for these sets of parameters**.** We found that The effect of wall waviness on u It is found that higher the dilation of the channel walls smaller the axial velocity in the flow region. The effect of dissipation u is Higher the dissipative heat smaller u in the flow region. With respect to the buoyancy ratio N, it is found that when the molecular buoyancy force dominates over the thermal buoyancy force |u| enhances irrespective of the directions of the buoyancy forces.

2. Methodology

We consider the motion of a viscous, incompressible fluid through a porous medium in a vertical wavy channel bounded by wavy walls (as shown in Figure 1). The thermal buoyancy in the flow field is created by a traveling thermal wave imposed on the boundary wall at $y = Lf(mx)$ while the boundary at $y = -Lf(mx)$ is maintained at constant temperature T_1. The walls are maintained at constant concentrations. A uniform magnetic field of strength H_o is applied transverse to the walls. Assuming the magnetic Reynolds to be small we neglect the induced magnetic field in comparison to the applied magnetic field. Assuming that the flow takes place at low concentration we neglect the Duffor effect. The Boussinesq approximation is used so that the density variations will be considered only in the buoyancy force. The viscous and Darcy dissipations are taken into account to the transport of heat by conduction and convection in the energy equation. Also the kinematic viscosity ν, the thermal conductivity k are treated as constants. We choose a rectangular Cartesian system 0 (x, y) with x-axis in the vertical direction and y-axis normal to the walls. The walls of the channel are at $y = \pm Lf(mx)$.

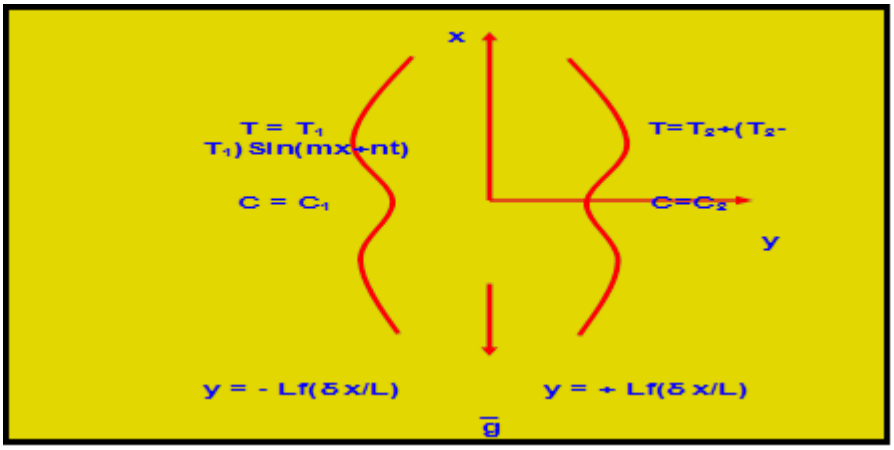

Fig. 1. Schematic diagram of the flow

The governing equations of the unsteady flow and heat transfer are:

Equation of continuity:

$$\frac{\partial u}{\partial x}+\frac{\partial v}{\partial y}=0 \tag{1}$$

Equation of linear momentum:

$$\rho_e\left(\frac{\partial u}{\partial t}+u\frac{\partial u}{\partial x}+v\frac{\partial u}{\partial y}\right)=-\frac{\partial p}{\partial x}+\mu\left(\frac{\partial^2 u}{\partial x^2}+\frac{\partial^2 u}{\partial y^2}\right)-\rho g-(\sigma\mu_e^2 H_{o)}^2 u \tag{2}$$

$$\rho_e\left(\frac{\partial v}{\partial t}+u\frac{\partial v}{\partial x}+v\frac{\partial v}{\partial y}\right)=-\frac{\partial p}{\partial y}+\mu\left(\frac{\partial^2 v}{\partial x^2}+\frac{\partial^2 v}{\partial y^2}\right) \tag{3}$$

Equation of energy:

$$\rho_e C_p\left(\frac{\partial T}{\partial t}+u\frac{\partial T}{\partial x}+v\frac{\partial T}{\partial y}\right)=$$
$$\lambda\left(\frac{\partial^2 T}{\partial x^2}+\frac{\partial^2 T}{\partial y^2}\right)+Q+\mu\left(\left(\frac{\partial u}{\partial y}\right)^2+\left(\frac{\partial v}{\partial x}\right)^2\right)+\left(\frac{\mu}{K}+\sigma\mu_e^2 H_o^2\right)(u^2+v^2)+Q_1^{'}(C-C_e) \tag{4}$$

Equation of Diffusion:

$$\left(\frac{\partial C}{\partial t}+u\frac{\partial C}{\partial x}+v\frac{\partial C}{\partial y}\right)=D_1\left(\frac{\partial^2 C}{\partial x^2}+\frac{\partial^2 C}{\partial y^2}\right)-k_1(C-C_e) \tag{5}$$

Equation of state:

$$\rho-\rho_e=-\beta\rho_e(T-T_e)-\beta^*\rho_e(C-C_e) \tag{6}$$

where ρ_e is the density of the fluid in the equilibrium state, T_e and Ce are the temperature and concentration in the equilibrium state, (u, v) are the velocity components along O (x, y) directions, p is the pressure, T and C are the temperature and concentration in the flow region, ρ is the density of the fluid, μ is the constant coefficient of viscosity, C_p is the specific heat at constant pressure, λ is the coefficient of thermal conductivity, k is the permeability of the porous medium, D_1 is the molecular diffusivity, $Q_1^{'}$ is the radiation absorption coefficient, β is the coefficient of thermal expansion, β^* is the volume expansion with mass fraction, k_1 is the chemical reaction coefficient, Q is the strength of the constant internal heat source, σ is electrical conductivity of the medium, μ_e is magnetic permeability and q_r is the radiative heat flux.

In the equilibrium state:

$$0 = -\frac{\partial p_e}{\partial x} - \rho_e g \tag{7}$$

where $p = p_e + p_D, p_D$ being the hydrodynamic pressure.

The flow is maintained by a constant volume flux for which a characteristic velocity is defined as:

$$q = \frac{1}{L}\int_{-Lf}^{Lf} u \, d\, y \tag{8}$$

The boundary conditions for the velocity and temperature fields are:

$$\begin{aligned} &u = 0,\ v = 0,\ T = T_1,\ C = C_1 \text{ on } y = +Lf\,(mx) \\ &u = 0,\ v = 0, T = T_2 + \Delta T_e\, Sin(mx + nt),\ C = C_2 \text{ on } y = -Lf\,(mx) \end{aligned} \tag{9}$$

where $\Delta T_e = T_2 - T_1$ and $Sin(mx + nt)$ is the imposed traveling thermal wave

In view of the continuity equation we define the stream function ψ as:

$$u = -\psi_y,\ v = \psi_x \tag{10}$$

Eliminating pressure, p from Eq. (2) and (3) and using the governing equations of the flow in terms of ψ are:

$$\begin{aligned} &[(\nabla^2\psi)_t + \psi_x(\nabla^2\psi)_y - \psi_y(\nabla^2\psi)_x] = \\ &\nu\nabla^4\psi - \beta g(T - T_0)_y - \beta^{\bullet} g(C - C_0)_y - \left(\frac{\sigma\mu_e^2 H_o^2}{\rho_e}\right)\frac{\partial^2\psi}{\partial y^2} \end{aligned} \tag{11) - (12}$$

$$\left(\frac{\partial C}{\partial t} - \frac{\partial\psi}{\partial y}\frac{\partial C}{\partial x} + \frac{\partial\psi}{\partial x}\frac{\partial C}{\partial y}\right) = D_1\nabla^2 C - k_1 C \tag{13}$$

Introducing the non-dimensional variables in Eq. (11) – (13) as:

$$x' = mx,\ y' = y/L, t' = t\nu m^2, \Psi' = \Psi/\nu, \theta = \frac{T - T_e}{\Delta T_e}, C' = \frac{C - C_2}{C_1 - C_2} \tag{14}$$

The governing equations in the non-dimensional form (after dropping the dashes) are:

$$\delta R(\delta(\nabla_1^2\psi)_t + \frac{\partial(\psi, \nabla_1^2\psi)}{\partial(x,y)}) = \nabla_1^4\psi - (\frac{G}{R})(\theta_y + NC_y) - M^2\frac{\partial^2\psi}{\partial y^2} \tag{15}$$

The energy equation in the non-dimensional form is:

$$\begin{aligned}&\delta P(\delta\frac{\partial\psi}{\partial t} - \frac{\partial\psi}{\partial y}\frac{\partial\theta}{\partial x} + \frac{\partial\psi}{\partial x}\frac{\partial\theta}{\partial y}) = \\ &\nabla_1^2\theta + \alpha + (\frac{PR^2E_c}{G})((\frac{\partial^2\psi}{\partial y^2})^2 + \delta^2(\frac{\partial^2\psi}{\partial x^2})^2) + (D^{-1} + M^2)(\delta^2(\frac{\partial\psi}{\partial x})^2 + (\frac{\partial\psi}{\partial y})^2)) + Q_1C\end{aligned} \tag{16}$$

The Diffusion equation is:

$$\delta Sc(\delta\frac{\partial C}{\partial t} - \frac{\partial\psi}{\partial y}\frac{\partial C}{\partial x} + \frac{\partial\psi}{\partial x}\frac{\partial C}{\partial y}) = \nabla_1^2 C - kC \tag{17}$$

where:

$R = \frac{qL}{\nu}$: Reynolds number

$G = \frac{\beta g\Delta T_e L^3}{\nu^2}$: Grashof number

$\mathrm{P} = \frac{\mu C_p}{k_1}$: Prandtl number

$E_c = \frac{\beta g L^3}{C_p}$: Eckert number

$\delta = mL$: Aspect ratio

$Sc = \frac{\nu}{D_1}$: Schmidt Number

$N = \frac{\beta^*\Delta C}{\beta\Delta T}$: Buoyancy Ratio

$\gamma = \frac{n}{\nu m^2}$: non-dimensional thermal wave velocity

$Q_1 = \frac{Q_1'(C_2 - C_1)L^2}{(T_2 - T_1)k_1C_p}$: Radiation absorption parameter

$M^2 = \frac{\sigma\mu_e^2H_o^2L^2}{\nu^2}$: Hartmann Number

$k = \frac{k_1L^2}{D_1}$: Chemical reaction parameter

$\alpha = \frac{QL^2}{(T_2 - T_1)k_1C_p}$: Heat source parameter

$\nabla_1^2 = \delta^2\frac{\partial^2}{\partial x^2} + \frac{\partial^2}{\partial y^2}$

The corresponding boundary conditions are:

$$\psi(+1)-\psi(-1)=-1,\ \frac{\partial\psi}{\partial x}=0,\ \ \frac{\partial\psi}{\partial y}=0 \quad at\ y=\pm 1 \tag{18}$$

$\theta(x,y)=1$, $C(x,y)=0$ on y = -1
$\theta(x,y)=Sin(x+\gamma t)$, C(x, y) = 1 on y = 1

$$\frac{\partial\theta}{\partial y}=0,\frac{\partial C}{\partial y}=0\ at\ y=0 \tag{19}$$

The value of ψ on the boundary assumes the constant volumetric flow in consistent with the hypothesis Eq. (8). Also the wall temperature varies in the axial direction in accordance with the prescribed arbitrary function t.

3. Analysis of The Flow

The main aim of the analysis is to discuss the perturbations created over a combined free and forced convection flow due to traveling thermal wave imposed on the boundaries.

Introducing the transformation:

$$\eta=\frac{y}{f(x)} \tag{20}$$

The equations (15) – (17) reduce to:

$$\delta R(\delta(F^2\psi)_t+\frac{\partial(\psi,F^2\psi)}{\partial(x,\eta)})=F^4\psi-(\frac{G}{R})(\theta_y+NC_y)-(M^2f^2)\frac{\partial^2\psi}{\partial\eta^2} \tag{21}$$

$$\begin{aligned}&\delta P(\delta f^2\frac{\partial\psi}{\partial t}+f(-\frac{\partial\psi}{\partial\eta}\frac{\partial\theta}{\partial x}+\frac{\partial\psi}{\partial x}\frac{\partial\theta}{\partial\eta}))=F^2\theta+\alpha f^2+(\frac{PR^2E_c}{G})((\frac{\partial^2\psi}{\partial\eta^2})^2\\&+\delta^2f^2(\frac{\partial^2\psi}{\partial x^2})^2)+(f^2(D^{-1}+M^2))(\delta^2(\frac{\partial\psi}{\partial x})^2+(\frac{\partial\psi}{\partial\eta})^2))+(Q_1f^2)C\end{aligned} \tag{22}$$

$$\delta Sc(\delta f^2\frac{\partial C}{\partial t}+f(-\frac{\partial\psi}{\partial\eta}\frac{\partial C}{\partial x}+\frac{\partial\psi}{\partial x}\frac{\partial C}{\partial\eta}))=F^2C-(kScf^2)C \tag{23}$$

where

$$F^2=\frac{\partial^2}{\partial\eta^2}+\delta^2\frac{\partial^2}{\partial x^2}$$

The perturbation analysis is carried out by assuming the aspect ratio δ to be small. We adopt the perturbation scheme and write:

$$\psi(x,\eta,t)=\psi_0(x,\eta,t)+\delta\psi_1(x,\eta,t)+\delta^2\psi_2(x,\eta,t)+\ldots\ldots\ldots$$
$$\theta(x,\eta,t)=\theta_0(x,\eta,t)+\delta\theta_1(x,\eta,t)+\delta^2\theta_2(x,\eta,t)+\ldots\ldots\ldots$$
$$C(x,\eta,t)=C_0(x,\eta,t)+\delta C_1(x,\eta,t)+\delta^2 C_2(x,\eta,t)+\ldots\ldots\ldots \quad (24)$$

On substituting (24) in (21) - (23) and separating the like powers of δ the equations and respective conditions to the zeroth order are:

$$\psi_{0,\eta\eta\eta\eta}-(M_1^2 f^2)\psi_{0,\eta\eta y}=\left(\frac{Gf^3}{R}\right)(\theta_{0,\eta}+NC_{O,\eta}) \quad (25)$$

$$\theta_{o,y\eta\eta}+(\alpha f^2)+\frac{PE_cR^2}{G}(\psi_{o,\eta\eta})^2+\frac{PE_cM_1^2}{G}(\psi_{o,\eta}^2)+Q_1C_0=0 \quad (26)$$

$$C_{O,\eta\eta}-(kScf^2)C_0=0 \quad (27)$$

with

$\psi_0(+1) - \Psi(-1) = -1$,
$\psi_{0,\eta}= 0$, $\psi_{0,x}=0$ at $\eta = \pm 1$

$$\theta_o=1 \ , C_0=0 \ \ on \ \ \eta=-1 \quad (28)$$

$$\theta_o=Sin(x+\gamma t), C_0=1 \ \ on\ \eta=1 \quad (29)$$

And to the first order are:

$$\psi_{1,,\eta\eta\eta\eta}-(M_1^2 f^2)\psi_{1,\eta\eta y}=\left(\frac{Gf^3}{R}\right)(\theta_{1,Y\eta}+NC_{1,\eta})+f(\psi_{0,\eta}\psi_{0,x\eta\eta y}-\psi_{0,x}\psi_{0,\eta\eta\eta}) \quad (30)$$

$$\theta_{1,\eta\eta}=f(\psi_{0,x}\theta_{o,\eta}-\psi_{0,\eta}\theta_{ox})+\frac{2PE_cR^2}{G}(\psi_{0,\eta\eta}.\psi_{1,yy})+\ +\frac{2PE_cM_1^2}{G}(\psi_{0,\eta}.\psi_{1,\eta})+Q_1C_1 \quad (31)$$

$$C_{1,\eta\eta}-(kScf^2)C_1=f(\psi_{0,x}C_{o,\eta}-\psi_{0,\eta}C_{ox}) \quad (32)$$

With

$\psi_{1(+1)} - \psi_{1(-1)} = 0$

$\psi_{1,y} = 0$, $\psi_{1,x} = 0$ at $\eta = \pm 1$ (33)
$\theta_1(\pm 1) = 0$, $C_1(\pm 1) = 0$ at $\eta = \pm 1$ (34)

Assuming Ec<<1 to be small we take the asymptotic expansions as:

$$\psi_0(x,\eta,t)=\psi_{00}(x,\eta,t)+Ec\,\psi_{01}(x,\eta,t)+\ldots\ldots\ldots$$
$$\psi_1(x,\eta,t)=\psi_{10}(x,\eta,t)+Ec\,\psi_{11}(x,\eta,t)+\quad\ldots\ldots\ldots$$
$$\theta_0(x,\eta,t)=\theta_{00}(x,\eta,t)+\theta_{01}(x,\eta,t)+\ldots\ldots\ldots\ldots$$
$$\theta_1(x,\eta,t)=\theta_{10}(x,\eta,t)+\theta_{11}(x,\eta,t)+\ldots\ldots\ldots\ldots$$
$$C_0(x,\eta,t)=C_{00}(x,\eta,t)+C_{01}(x,\eta,t)+\ldots\ldots\ldots\ldots$$
$$C_1(x,\eta,t)=C_{10}(x,\eta,t)+C_{11}(x,\eta,t)+\ldots\ldots\ldots\ldots$$

Substituting the expansions Eq. (28) in Eq. (25) - (28) and separating the like powers of E_c we get the following:

$$\theta_{00,\eta\eta}=-(\alpha f^2),\quad \theta_{00}(-1)=1,\theta_{00}(+1)=SinD_1 \tag{35}$$

$$C_{00,\eta\eta}(kScf^2)C_{00}=0,\quad C_{00}(-1)=0,C_{00}(+1)=1 \tag{36}$$

$$\psi_{00,\eta\eta\eta\eta}-(M_1^2f^2)\psi_{00,\eta\eta}=(\frac{Gf^3}{R})(\theta_{00,\eta}+NC_{00,\eta}),$$
$$\psi_{00}(+1)-\psi_{00}(-1)=1,\psi_{00,y}=0,\psi_{00,x}=0\ \ at\ \eta=\pm1 \tag{37}$$

$$\theta_{01,\eta\eta}=-\frac{PR}{G}\psi^2{}_{00,\eta\eta}-\frac{PM_1^2}{G}\psi_{00,\eta}^2\qquad,\quad \theta_{01}(\pm1)=0 \tag{38}$$

$$C_{01,yy}-(kSc)C_{01}=0,\quad C_{01}(-1)=0,C_{01}(+1)=0 \tag{39}$$

$$\psi_{01,\eta\eta\eta\eta}-(M_1^2f^2)\psi_{01,\eta\eta}=(\frac{Gf^3}{R})(\theta_{01,\eta}+NC_{01,\eta})$$
$$\psi_{01}(+1)-\psi_{01}(-1)=0,\psi_{01,\eta}=0,\psi_{01,x}=0\ \ at\ \eta=\pm1 \tag{40}$$

$$\theta_{10,\eta\eta}=GP(\psi_{00,\eta}\theta_{00,x}-\psi_{00,x}\theta_{00,\eta})\qquad\theta_{10}(\pm1)=0 \tag{41}$$

$$C_{10,\eta\eta}-(kSc)C_{10}=Sc(\psi_{00,\eta}C_{00,x}-\psi_{00,x}C_{00,\eta})C_{10}(\pm1)=0 \tag{42}$$

$$\psi_{10,\eta\eta\eta\eta}-(M_1^2f^2)\psi_{10,\eta\eta}=\frac{G}{R}(\theta_{10,\eta}+NC_{10,\eta})++(\psi_{00,\eta}\psi_{00,x\eta\eta}-\psi_{00,x}\psi_{00,\eta\eta\eta})$$
$$\psi_{10}(+1)-\psi_{10}(-1)=0,\psi_{10,\eta}=0,\psi_{10,x}=0\ \ at\ \eta=\pm1 \tag{43}$$

$$\theta_{11,\eta\eta}=P(\psi_{00,\eta}\theta_{01,x}-\psi_{01,x}\theta_{00,\eta}+\theta_{00,x}\psi_{01,\eta}$$
$$-\theta_{01,y}\psi_{0,x})-\frac{2PR^2}{G}\psi_{00,\eta\eta}\psi_{10,\eta\eta}-\frac{2PM_1^2}{G}\psi_{00,\eta}\psi_{10,\eta}\ ,\ \theta_1(\pm1)=0 \tag{44}$$

$$C_{11,\eta\eta}-(kSc)C_{11}=Sc(\psi_{00,\eta}C_{01,x}-\psi_{01,x}C_{00,\eta}+C_{00,x}\psi_{01,\eta}-C_{01,\eta}\psi_{0,x}) \tag{45}$$

$$\psi_{11,\eta\eta\eta\eta}-(M_1^2 f^2)\psi_{1,\eta\eta}=\frac{G}{R}(\theta_{11,\eta}+NC_{11,\eta})+(\psi_{00,\eta}\psi_{11,x\eta\eta}-$$
$$-\psi_{00,x}\psi_{01,\eta\eta\eta}+\psi_{01,\eta}\psi_{00,x\eta\eta}-\psi_{01.x}\psi_{00,\eta\eta\eta}) \quad (46)$$
$$\psi_{11}(+1)-\psi_{11}(-1)=0,\psi_{11,\eta}=0,\psi_{11,x}=0 \ \ at\ \eta=\pm 1$$

4. Solution of The Problem

Solving the equations (35) – (46) subject to the relevant boundary conditions we obtain:

$$\theta_{oo}(y,t)=(\frac{\alpha}{2})(1-\eta^2)+(\frac{Sin(D_1)-1}{2})y+(\frac{Sin(D_1)+1}{2})-\frac{Q_1}{2\beta_1^2}(1-\frac{Cosh(\beta_1\eta)}{Cosh(\beta_1)})+\frac{Q_1}{2\beta_1^2}(\eta-\frac{Sinh(\beta_1\eta)}{Sinh(\beta_1)})$$

$$C_{00}=0.5(\frac{Cosh(\beta_1 y)}{Cosh(\beta_1)}-\frac{Sinh(\beta_1 y)}{Sinh(\beta_1)})$$

$$\theta_{01}(y,t)=a_{31}(\eta^2-1)+a_{34}(Sh(2\beta_1 y)-Sh(2\beta_1))+(a_{32})(Ch(2\beta_2\eta)--Ch(2\beta_2))+(a_{33})(Ch(2\beta_1 y)$$
$$-Ch(2\beta_1))+a_{35}(Sh(2\beta_2 y)-Sh(2\beta_2))-(\frac{2a_{24}}{M_1^3}))(Ch(M_1 y)-Ch(M_1))+(a_{38}+(a_{36}+a_{39})\eta)(Ch(\beta_1 y)$$
$$-Ch(\beta_1))+a_{37}(\eta Sh(2\beta_1 y)-Sh(2\beta_1))+(a_{40})(Sh(\beta_1 y)-Sh(\beta_1))+a_{41}(Ch(\beta_2\eta)-Ch(\beta_2))$$
$$+a_{42}(Ch(\beta_3\eta)-Ch(\beta_3))+a_{43}(Ch(\beta_4\eta)-Ch(\beta_4))+a_{44}(Sh(\beta_3\eta)-\eta Sh(\beta_3))+a_{45}(Sh(\beta_4\eta)-\eta Sh(\beta_4))$$

$$\psi_{01}(\eta,t)=a_{68}+a_{67}\eta+a_{65}Ch(\beta_2\eta)+a_{66}Sh(\beta_2\eta)+\phi_2(\eta)$$
$$\phi_2(\eta)=-a_{47}\eta^2+a_{48}\eta^3+a_{49}\eta^5-a_{50}Sh(2\beta_1\eta)-a_{51}Ch(2\beta_1\eta)-a_{52}\eta Ch(2\beta_2\eta)+a_{53}\eta^2 Sh(\beta_2\eta)$$
$$+a_{54}\eta^2 Sh(\beta_1\eta)+a_{55}\eta Ch(\beta_2\eta)+a_{56}\eta Ch(\beta_1\eta)+a_{57}Sh(\beta_1\eta)-a_{58}Ch(\beta_1\eta)-a_{59}\eta Sh(\beta_2\eta)-a_{60}$$
$$\eta^2 Sh(\beta_1\eta)-a_{61}Sh(\beta_3\eta)-a_{62}Sh(\beta_4\eta)-a_{63}Ch(\beta_3\eta)-a_{64}Ch(\beta_4\eta)$$

$$C_{10}(y,t) = b_1(\eta^4 - 1)Sh(\beta_1\eta) + b_2(\eta^4 - 1)Ch(\beta_1\eta) + b_3(\eta^3 Ch(\beta_1\eta) - Ch(\beta_1)\frac{Sh(\beta_1\eta)}{Sh(\beta_1)}) + b_4(\eta^3 Sh(\beta_1\eta)$$
$$- Sh(\beta_1)\frac{Ch(\beta_1\eta)}{Ch(\beta_1)}) + b_5(\eta^2 Sh(2\beta_1\eta) - Sh(2\beta_1)\frac{Sh(\beta_1\eta)}{Sh(\beta_1)}) + b_6(\eta Ch(2\beta_1\eta) - Ch(2\beta_1)\frac{Sh(\beta_1\eta)}{Sh(\beta_1)}) +$$
$$b_7(\eta^2 Sh(\beta_3\eta) - Sh(\beta_3)\frac{Sh(\beta_1\eta)}{Sh(\beta_1)}) + b_8(\eta^2 Sh(\beta_4\eta) - Sh(\beta_4)\frac{Sh(\beta_1\eta)}{Sh(\beta_1)}) + b_9(\eta^2 Ch(\beta_3\eta) -$$
$$Ch(\beta_3)\frac{Ch(\beta_1\eta)}{Ch(\beta_1)}) + b_{10}(\eta^2 Ch(\beta_4\eta) - Ch(\beta_4)\frac{Ch(\beta_1\eta)}{Ch(\beta_1)}) + b_{11}(\eta Ch(\beta_3\eta) - Ch(\beta_3)\frac{Sh(\beta_1\eta)}{Sh(\beta_1)}) +$$
$$b_{12}(\eta Ch(\beta_4\eta) - Ch(\beta_4)\frac{Sh(\beta_1\eta)}{Sh(\beta_1)}) + b_{13}(\eta Sh(\beta_3\eta) - Sh(\beta_3))) + b_{14}(\eta Sh(\beta_4\eta) - Sh(\beta_4)) +$$
$$b_{15}(\eta^2 Ch(2\beta_1\eta) - Ch(2\beta_1)\frac{Ch(\beta_1\eta)}{Ch(\beta_1)}) + b_{16}(\eta Sh(2\beta_1\eta) - Sh(2\beta_1)) + b_{17}(\eta Ch(\beta_1\eta) - Ch(\beta_1)\frac{Sh(\beta_1\eta)}{Sh(\beta_1)}) +$$
$$b_{20}(\eta^2 - 1)Sh(\beta_1\eta) + b_{23}(\eta Sh(\beta_1\eta) - Sh(\beta_1)) + b_{24}(\eta Ch(\beta_1\eta) - Ch(\beta_1)\frac{Sh(\beta_1\eta)}{Sh(\beta_1)}) + b_{25}(Sh(\beta_3\eta) -$$
$$Sh(\beta_3)\frac{Sh(\beta_1\eta)}{Sh(\beta_1)}) + b_{26}(Sh(\beta_4\eta) - Sh(\beta_4)\frac{Sh(\beta_1\eta)}{Sh(\beta_1)}) + b_{27}(Ch(\beta_3\eta) - Ch(\beta_3)\frac{Ch(\beta_1\eta)}{Ch(\beta_1)}) + b_{28}(Ch(\beta_4\eta) -$$
$$Ch(\beta_4)\frac{Ch(\beta_1\eta)}{Ch(\beta_1)}) + b_{29}(Ch(2\beta_1\eta) - Ch(2\beta_1)) + b_{30}(Sh(2\beta_1\eta) - Sh(2\beta_1)\frac{Sh(\beta_1\eta)}{Sh(\beta_1)})$$

$$\theta_{10}(y,t) = d_2\eta^2 + d_3\eta^3 + d_4\eta^4 + d_5\eta^5 + (d_6 + d_{10}\eta + d_{14}\eta^2)Sh(\beta_3\eta) + (d_7 + d_{11}\eta + d_{15}\eta^2)Sh(\beta_4\eta)$$
$$+ (d_8 + d_{12}\eta + d_{16}\eta^2)Ch(\beta_3\eta) + (d_9 + d_{13}\eta + d_{17}\eta^2)Ch(\beta_4\eta) + (d_{18} + d_{20}\eta + d_{22}\eta^2 + d_{24}\eta^3 +$$
$$+ d_{26}\eta^4)Ch(\beta_1\eta) + (d_{21}\eta + d_{23}\eta^2 + d_{54}\eta^3 + d_{27}\eta^4)Sh(\beta_1\eta) + (d_{28} + d_{30}\eta + d_{32}\eta^2)Sh(2\beta_1\eta) +$$
$$+ (d_{29} + d_{31}\eta)Ch(2\beta_1\eta) + (d_{33} + d_{35}\eta + d_{37}\eta^2)Sh(\beta_2\eta) + (d_{34} + d_{36}\eta + d_{38}\eta^2)Ch(\beta_2\eta) +$$
$$+ d_{39}\eta + d_{40}$$

$$\psi_{10} = e_{78}Ch(\beta_2\eta) + e_{79}Sh(\beta_2\eta) + e_{80}\eta + e_{81} + \phi_4(y)$$
$$\phi_4(y) = e_{44}\eta + e_{45}\eta^2 + e_{46}\eta^3 + e_{47}\eta^4 + e_{48}\eta^6 + (e_{49} + e_{53}\eta)Ch(2\beta_2\eta) + (e_{50} + e_{54}\eta)Sh(2\beta_2\eta) +$$
$$+ (e_{52}\eta + e_{51})Sh(2\beta_1\eta) + e_{55}Ch(2\beta_1\eta) + (e_{56} + e_{62}\eta + e_{69}\eta^2)Ch(\beta_3\eta) + (e_{57} + e_{63}\eta +$$
$$+ e_{70}\eta^2)Ch(\beta_4\eta) + (e_{58} + e_{60}\eta)Sh(\beta_3\eta) + (e_{59} + e_{61}\eta + e_{71}\eta^2)Sh(\beta_4\eta) + (e_{64} +$$
$$+ (e_{68} + e_{72})\eta + e_{74}\eta^2 + e_{76}\eta^3)Ch(\beta_1\eta) + (e_{65} + e_{73}\eta^2 + e_{75}\eta^3 + e_{77}\eta^4)Sh(\beta_1\eta)$$
$$+ e_{66}Sh(\beta_2\eta) + e_{67}Ch(\beta_2\eta) +$$

Where $a_1, a_2, \ldots\ldots\ldots\ldots a_{105}, b_1, b_2, \ldots\ldots\ldots\ldots b_{79}$, are constants given in the appendix

0 and reduces with $\alpha>0$ in the heating case and in the cooling case it reduces at η = +1 with $\alpha>0$ and enhances it η = -1 with $\alpha<0$ (Table 12 and Table 17 Lesser the molecular diffusivity larger |Sh| at $\eta = \pm 1$. For higher $Q_1 \geq 2$, it enhances at η = +1 and reduces at η = -1.

5. Shear Stress, Nusselt Number and Sherwood Number

The shear stress on the channel walls is given by:

$$\tau = \mu\left(\frac{\partial u}{\partial y} + \frac{\partial v}{\partial x}\right)_{y=\pm L}$$

which in the non- dimensional form reduces to:

$$\tau = (\frac{\tau}{\frac{\mu U}{a}}) = (\psi_{yy} - \delta^2 \psi_{xx})$$
$$= [\psi_{00,yy} + Ec\,\psi_{01,yy} + \delta(\psi_{10,yy} + Ec\,\psi_{11,yy} + O(\delta^2)]_{y=\pm 1}$$

and the corresponding expressions are:

$$(\tau)_{y=+1} = b_{90} + \delta b_{91} + O(\delta^2)$$

$$(\tau)_{y=-1} = b_{92} + \delta b_{93} + O(\delta^2)$$

The local rate of heat transfer coefficient (Nusselt number Nu) on the walls has been calculated using the formula:

$$Nu = \frac{1}{\theta_m - \theta_w}(\frac{\partial \theta}{\partial y})_{y=\pm 1}$$

and the corresponding expressions are:

$$(Nu)_{y=+1} = \frac{(e_{84} + Ece_{86} + \delta e_{88})}{(\theta_m - Sin(D_1)}$$

$$(Nu)_{y=-1} = \frac{(e_{85} + Ece_{87} + \delta e_{89})}{(\theta_m - 1)}$$

$$\theta_m = e_{90} + Ece_{91} + \delta e_{92}$$

The local rate of mass transfer coefficient (Sherwood number) (Sh) on the walls has been calculated using the formula:

$$Sh = \frac{1}{C_m - C_w}(\frac{\partial C}{\partial y})_{y=\pm 1}$$

and the corresponding expressions are:

$$(Sh)_{y=+1} = \frac{(e_{93} + \delta e_{95})}{(C_m - 1)}$$

$$(Sh)_{y=-1} = \frac{(e_{94} + \delta e_{96})}{(C_m)}$$

$$C_m = e_{97} + \delta e_{98}$$

where e_1…….e_{98} are constants.

6. Solution of The Problem

Solving the equations (35)- (46) subject to the relevant boundary conditions we obtain

$$\theta_{oo}(y,t) = (\frac{\alpha}{2})(1-\eta^2) + (\frac{Sin(D_1)-1}{2})y + (\frac{Sin(D_1)+1}{2}) - \\ -\frac{Q_1}{2\beta_1^2}(1-\frac{Cosh(\beta_1\eta)}{Cosh(\beta_1)}) + \frac{Q_1}{2\beta_1^2}(\eta - \frac{Sinh(\beta_1\eta)}{Sinh(\beta_1)})$$

$$C_{00} = 0.5(\frac{Cosh(\beta_1 y)}{Cosh(\beta_1)} - \frac{Sinh(\beta_1 y)}{Sinh(\beta_1)})$$

$$\psi_{oo}(y,t) = a_{13}Cosh(M_1\eta) + a_{14}Sinh(M_1\eta) + a_{15}\eta + \phi_1(\eta)$$
$$\phi_1(\eta) = a_9 + a_{10}\eta^3 + a_{11}Cosh(\beta_1\eta) + a_{12}Sinh(\beta_1\eta)$$

7. Results and Discussion

We analyze the effect of radiation absorption, chemical reaction and dissipation on the unsteady convective heat and mass transfer flow of a viscous, electrically conducting fluid in a vertical wavy channel in the presence of heat source. The equations governing the flow, heat and mass transfer are solved by using a regular perturbation technique with the slope δ as a perturbation parameter.

The axial velocity (u) is exhibited in Figure 2 to Figure 10 for different values of G, R, M, β, N, Sc, k, Q, Ec, α and x+γt. The actual axial flow is in the vertically upward direction and hence u<0 represents a reversal flow. Figure 2 represents u with Grashof number G. It is found that u exhibits a reversal flow for G<0 and the region of reversal flow enlarges with increase in G<0. Also the magnitude of u enhances with increase in |G| with maximum |u| attained at η = 0. An increase in the Reynolds number R depreciates with increase in R. u exhibits a reversal flow at R = 140 (Figure 3). Figure 4 represents u with Hartmann number M. It is found that higher the Lorentz force larger the axial velocity. Figure 5 represents u with heat source parameter α. It is found that u exhibits a reversal flow with $\alpha \geq 4$. |u| depreciates with $\alpha \leq 4$ and enhances with higher $\alpha \geq 6$. Also u enhances with $|\alpha|$(<0). Figure 6 represents u with Sc and Q_1. u exhibits a reversal flow with higher Sc = 2.01. It is found that lesser the molecular diffusivity smaller |u| in the entire flow region. An increase in the radiation absorption Q_1 results in an enhancement in |u|. Figure 7 represents u with chemical reaction parameter k. It is found that u exhibits a reversal flow with higher values of k≥ 1.5 and the region of reversal flow enlarges with increase in k. Also |u| enhances with k in the entire flow region.

The effect of wall waviness on u is shown in Figure 8. It is found that higher the dilation of the channel walls smaller the axial velocity in the flow region. The effect of dissipation u is shown in Figure 9. Higher the dissipative heat smaller u in the flow region. With respect to the buoyancy ratio N, it is found that when the molecular buoyancy force dominates over the thermal buoyancy force |u| enhances irrespective of the directions of the buoyancy forces. Also u exhibits a reversal flow with |N| (<0). (Figure 10). Figure 11 represents u with the phase $x+\gamma t$ of the boundary temperature. It is found that the axial velocity depreciates with $x+\gamma t \leq \pi/2$, and enhances with higher $x+\gamma t = \pi$ and again depreciates with still higher $x+\gamma t = 2\pi$.

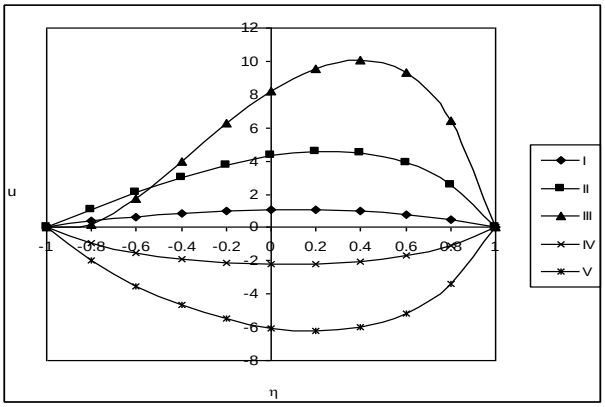

Fig. 2. Variation of u with G

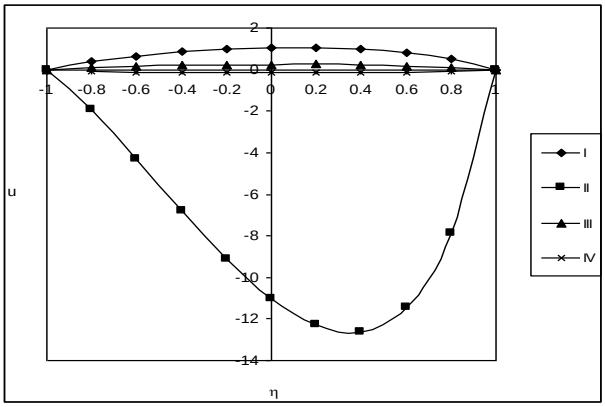

Fig. 3. Variation of u with R

	I	II	III	IV	V	VI		I	II	III
G	100	300	500	-100	-300	-500	R	35	70	140

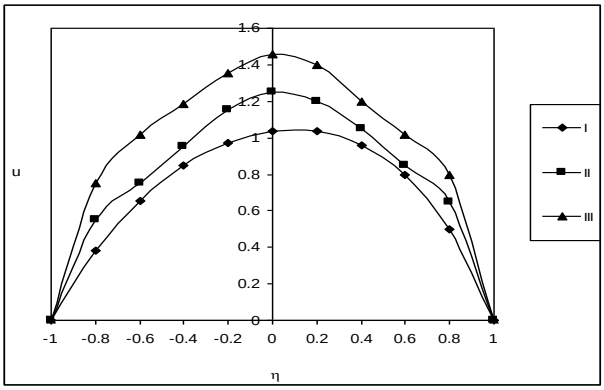

Fig. 4. Variation of u with M

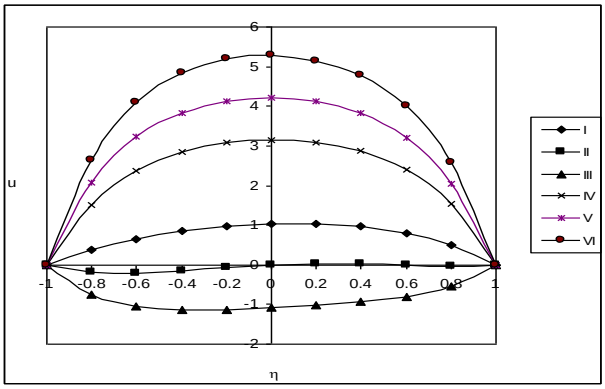

Fig. 5. Variation of u with α

	I	II	III		I	II	III	IV	V	VI
M	2	4	6	α	2	4	6	-2	-4	-6

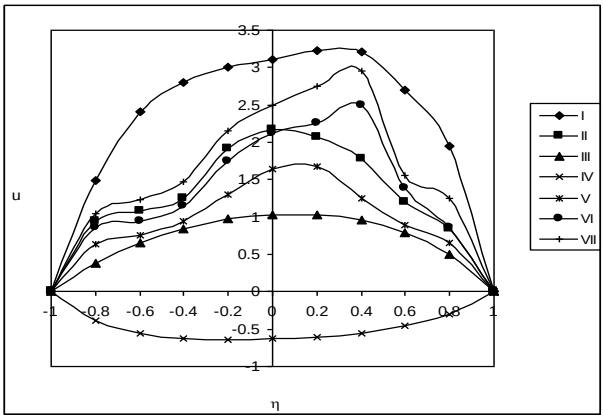

Fig. 6. Variation of u with Sc & Q_1

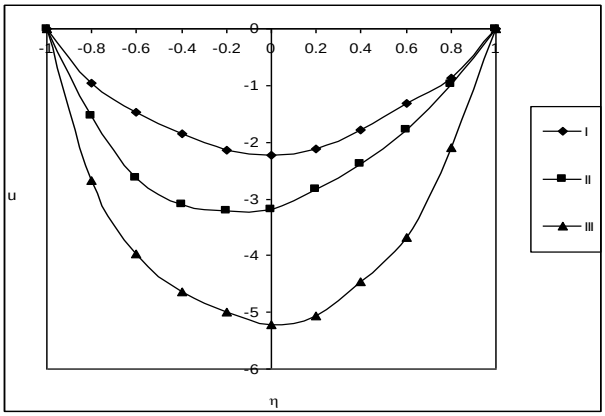

Fig. 7. Variation of u with k

	I	II	III	IV	V	VI	VII		I	II	III
Sc	0.24	0.6	1.3	2.01	1.3	1.3	1.3	k	0.5	1.5	2.5
Q_1	0.5	0.5	0.5	0.5	1	1.5	2				

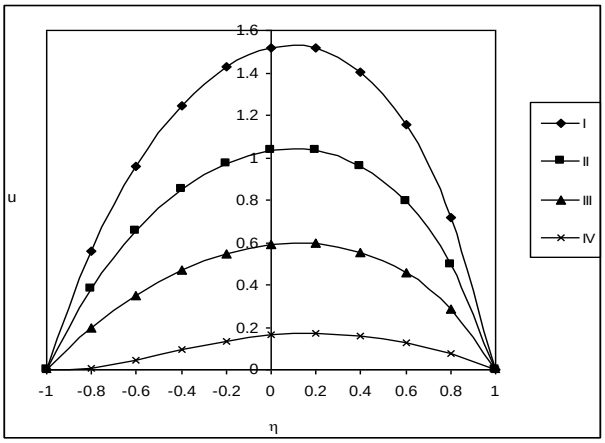

Fig. 8. Variation of u with β

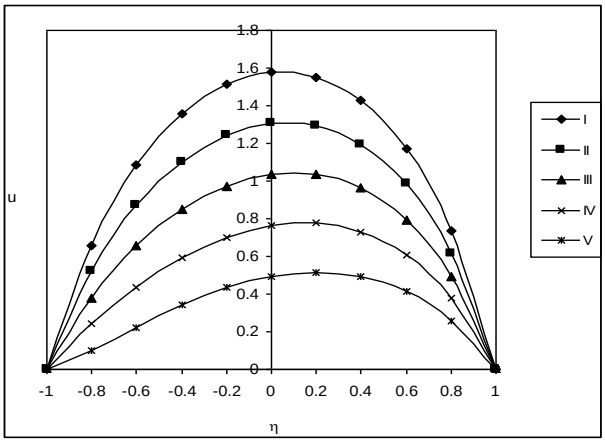

Fig. 9. Variation of u with E_c

	I	II	III	IV		I	II	III	IV	V
β	0.3	0.5	0.7	0.9	E_c	0.01	0.03	0.05	0.07	0.09

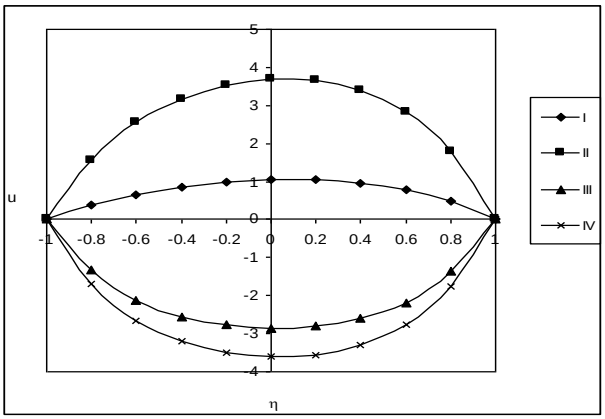

Fig. 10. Variation of u with N

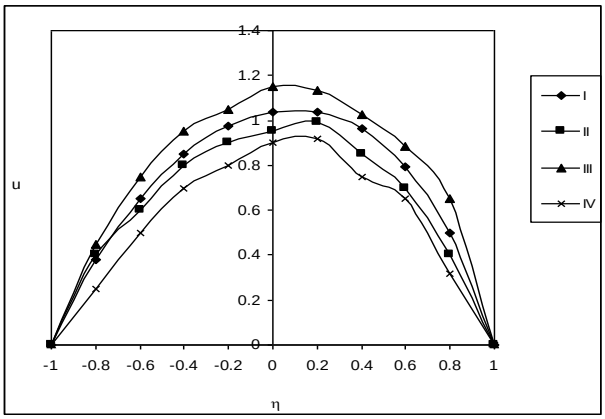

Fig. 11. Variation of u with x+γt

	I	II	III	IV		I	II	III	IV
N	1	2	-0.5	-0.8	x+γt	π/4	π/2	π	2π

The secondary velocity (v) which is due to the non-uniform boundary and boundary temperature is shown in Figure 12 to Figure 22 for different parametric values. Figure 12 represents v with G. It is found that v is towards the boundary for G>0 and is towards the midregion. |v| enhances with increase in G>0 and reduces with G<0 with maximum |v| attained at $\eta = 0$. The magnitude of v depreciates with R and enhances with increase in M (Figure 13 & Figure 14). From Figure 15 we find that the secondary velocity enhances with increase in $\alpha>0$ and depreciates with $|\alpha|(<0)$. From Figure 16, the variation of v with Sc shows that lesser the molecular diffusivity larger v and for further lowering of the molecular diffusivity smaller v in the flow region. |v| depreciates with increase in $Q_1 \leq 1$ and enhances with higher $Q_1 \geq 1.5$ (Figure 17). With respect to the buoyancy ratio N we find that the magnitude of v enhances with increase in |N| irrespective of the directions of the buoyancy forces (Figure 18). Figure 19 represents v with chemical reaction parameter k. It is found that higher the dissipative heat smaller |v| in the entire flow region. From Figure 20 it can be seen that |v| enhances with increase in β. Thus higher the dilation of the channel walls larger the secondary velocity in the flow region. The effect of dissipation on v is exhibited in Figure 21. Higher the dissipative heat larger v in the entire flow region. An increase in the phase $x+\gamma t \leq \pi$ depreciates |v| and enhances it for higher $x+\gamma t = 2\pi$ (Figure 22).

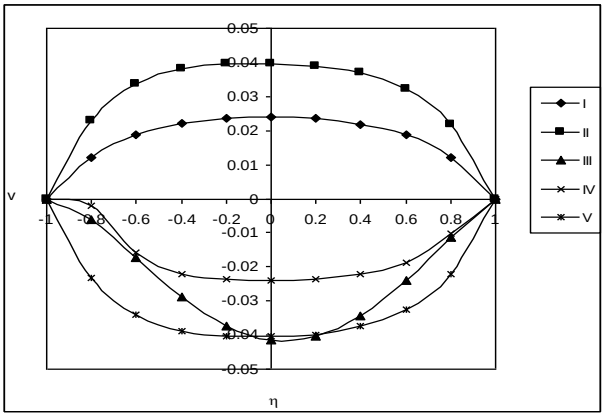

Fig. 12. Variation of v with G

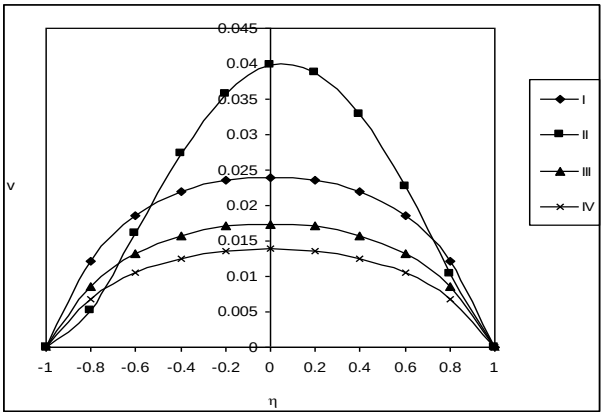

Fig. 13. Variation of v with R

	I	II	III	IV	V	VI		I	II	III
G	100	300	500	-100	-300	-500	R	35	70	140

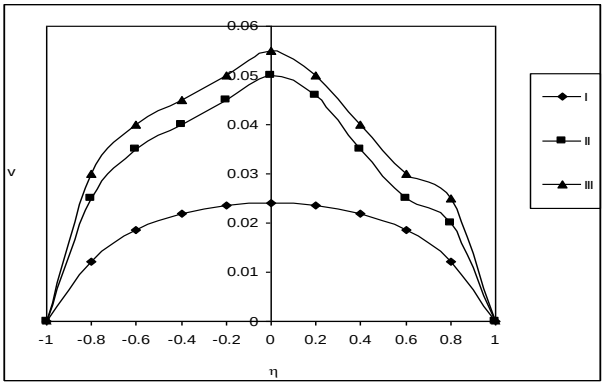

Fig. 14 Variation of v with M

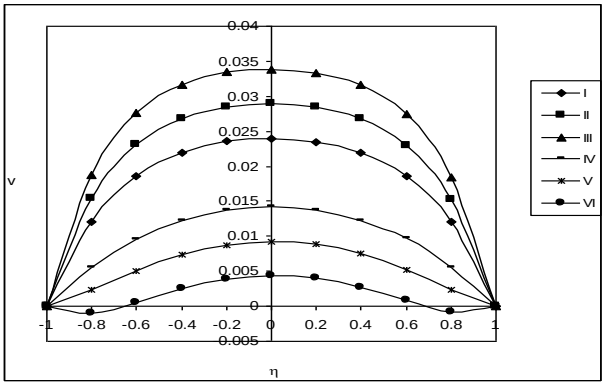

Fig. 15. Variation of v with α

	I	II	III		I	II	III	IV	V	VI
M	2	4	6	α	2	4	6	-2	-4	-6

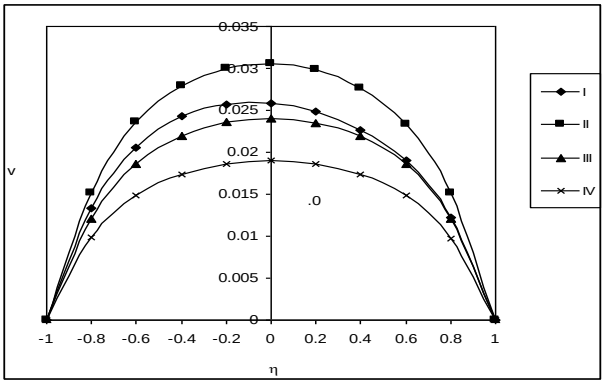

Fig. 16. Variation of v with Sc

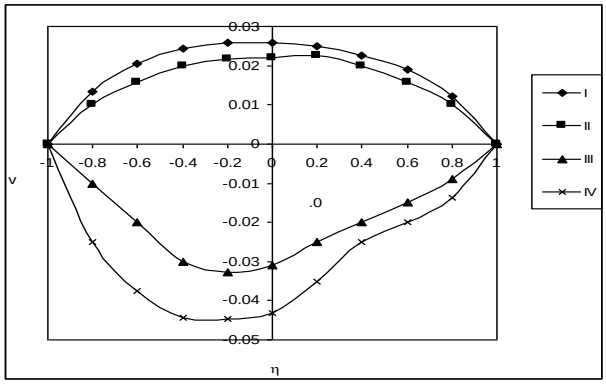

Fig. 17. Variation of v with Q_1

	I	II	III	IV		I	II	III	IV
Sc	0.24	0.6	1.3	2.01	Q_1	0.5	1	1.5	2.0

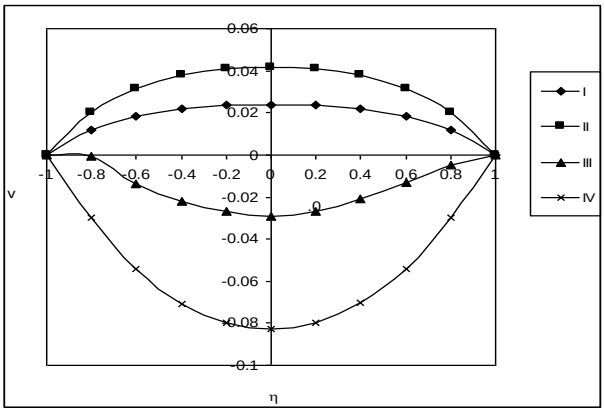

Fig. 18. Variation of v with N

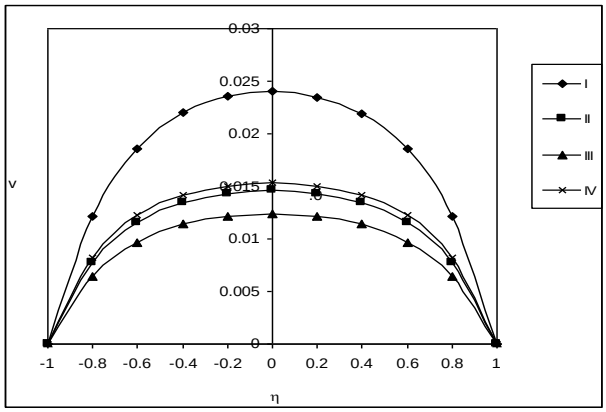

Fig. 19. Variation of v with k

	I	II	III	IV		I	II	III	IV
N	1	2	-0.5	2.0	k	0.5	1.5	2.5	3.5

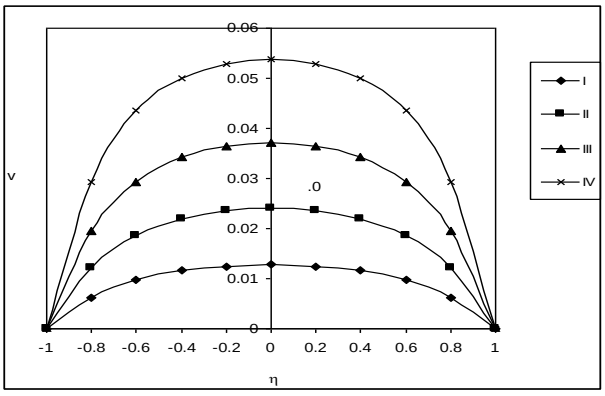

Fig. 20. Variation of v with β

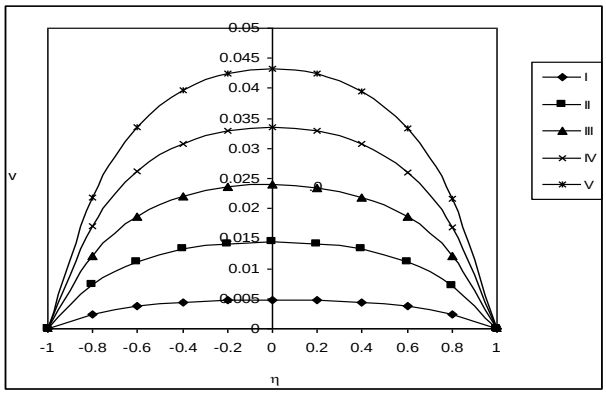

Fig. 21. Variation of v with E_c

	I	II	III	IV		I	II	III	IV	V
β	0.3	0.5	0.7	0.9	E_c	0.01	0.03	0.05	0.07	0.09

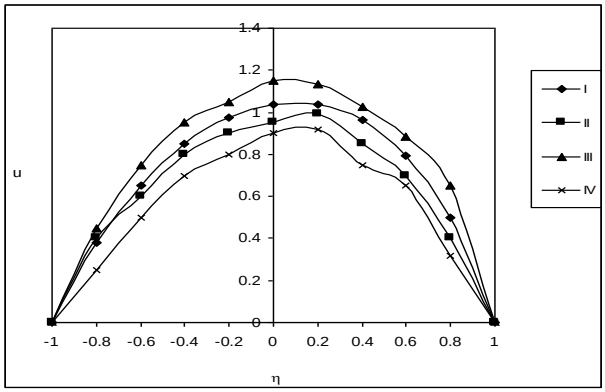

Fig. 22. Variation of v with x+γt

	I	II	III	IV
x+γt	π/4	π/2	π	2π

The non-dimensional temperature (θ) is shown in Figure 23 to Figure 32 for different parametric values. We follow the convention that the non-dimensional temperature is positive or negative according as the actual temperature is greater/lesser than the temperature T_2 on the right wall η = +1. Figure 23 represents θ with G. It is found that the actual temperature reduces with increase in |G| in the entire flow region. An increase in R reduces the actual temperature in flow region (Figure 24). With respect to M it can be seen that higher the Lorentz force smaller the actual temperature (Figure 25). The actual temperature enhances with increase in the strength of the heat source α and decreases with that of heat sink (Figure 26). With respect to Sc we find that lesser the molecular diffusivity larger the actual temperature and for further lowering of the molecular diffusivity smaller the actual temperature (Figure 27). From Figure 28 we find that an increase in Q_1 enhances the actual temperature in the left half and reduces in the right half of the channel. With respect to the chemical reaction parameter k, it can be seen that the actual temperature reduces with increase in k = 2.5, it enhances and for still higher k = 3.5, it reduces in the entire flow region (Figure 29). From Figure 30 we find that higher the dissipative heat smaller the actual temperature. The effect of wall waviness on θ is shown in Figure 31. It is found that higher the dilation of the channel walls larger the actual temperature. The actual temperature enhances with smaller and higher values of x+γt and depreciates with intermediate value of x+γt = π (Figure 32).

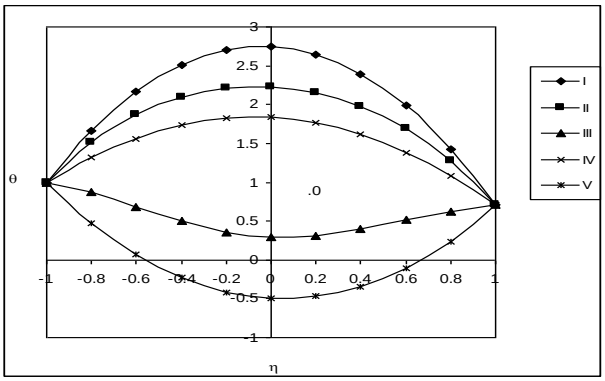

Fig. 23. Variation of θ with G

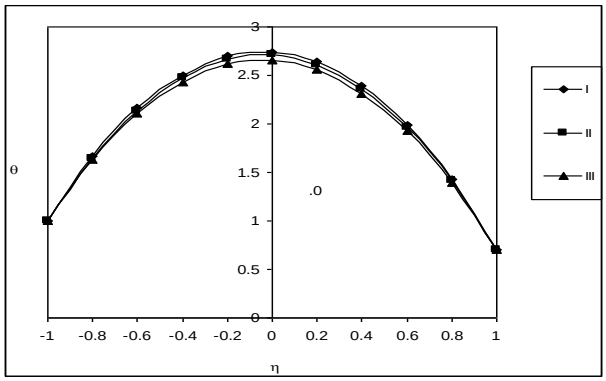

Fig. 24. Variation of θ with R

	I	II	III	IV	V	VI		I	II	III
G	100	300	500	-100	-300	-500	R	35	70	140

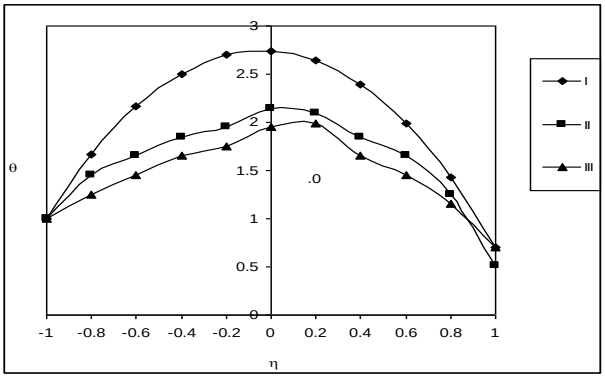

Fig. 25. Variation of θ with M

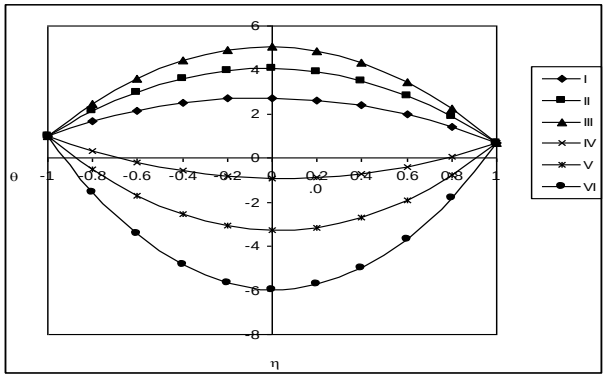

Fig. 26. Variation of θ with α

	I	II	III		I	II	III	IV	V	VI
M	2	4	6	α	2	4	6	-2	-4	-6

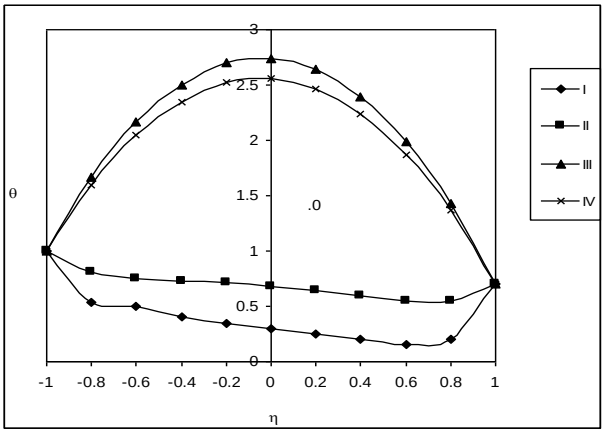

Fig. 27. Variation of θ with Sc

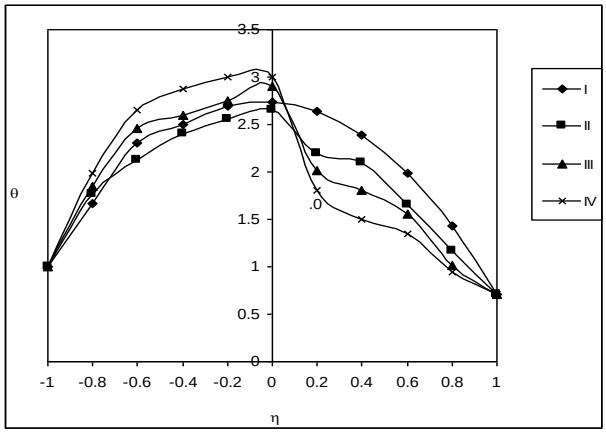

Fig. 28. Variation of θ with Q_1

	I	II	III	IV		I	II	III	IV
Sc	0.24	0.6	1.3	2.01	Q_1	0.5	1	1.5	2

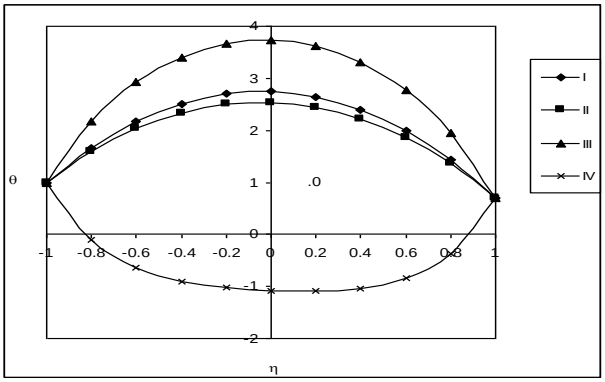

Fig. 29. Variation of θ with k

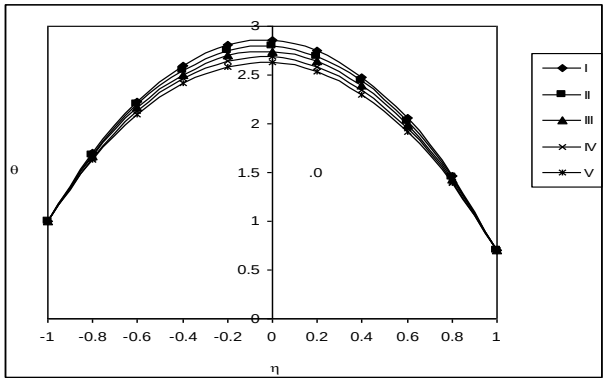

Fig. 30. Variation of θ with E_c

	I	II	III	IV		I	II	III	IV	V
k	0.5	1.5	2.5	3.5	E_c	0.01	0.03	0.05	0.07	0.09

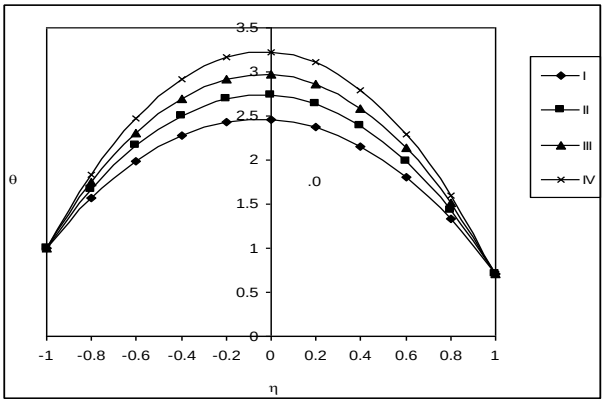

Fig. 31. Variation of θ with β

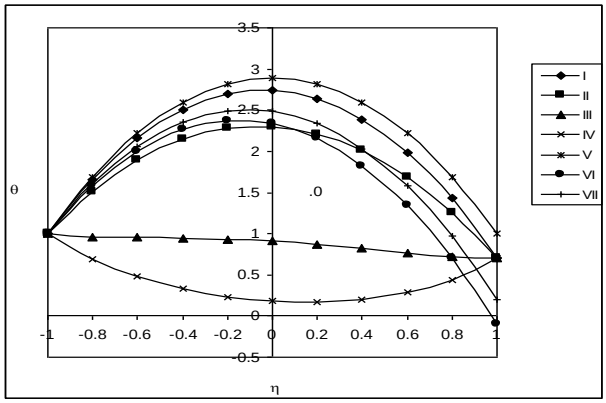

Fig. 32. Variation of θ with N & x+γt

	I	II	III	IV		I	II	III	IV	V	VI	VII
β	0.3	0.5	0.7	0.9	N	1	-0.5	0	-0	1	1	1
					x+γt	π/4	π/4	π/4	π/4	π/2	π	2π

The non-dimensional concentration (C) is exhibited in Figure 33 to Figure 43 for different parametric values. We follow the convention that the non-dimensional concentration is positive or negative according as the actual concentration is greater/lesser than the concentration on the right wall. Figure 33 represents C with G. It is found that the actual concentration enhances with increase in G>0 and reduces with |G| (<0). An increase in R reduces the actual concentration (Figure 34). The actual concentration enhances in the left half and depreciates in the right half of the channel with increase in M (Figure 35). From Figure 36 it can be seen that the actual concentration enhances with $\alpha>0$ and reduces with $|\alpha|$ (<0). With respect to Sc we find that lesser the molecular diffusivity larger the actual concentration in the left half and smaller in the higher half and for further lowering of the molecular diffusivity the region where the actual concentration is positive is confined for a narrow region adjacent to $\eta = -1$ (Figure 37). An increase in Q_1 enhances C in the left half and reduces in the right half of the channel (Figure 38). From Figure 39 it can be seen that the actual concentration reduces with increase in $k \leq 2.5$ and enhances with higher $k = 3.5$. The effect of wall waviness on C is shown in Figure 40. It can be seen that higher the dilation of the channel walls larger in the right half and smaller in the right half of the channel. With respect to the buoyancy ratio N we find that when the molecular buoyancy dominates over the thermal buoyancy force the actual concentration enhances when the buoyancy forces act in the same direction and for the forces acting in opposite directions, it depreciates in the entire flow region (Figure 41). The variation of C with Ec shows that higher the dissipative heat larger the actual concentration in the left half and smaller in the right half of the channel (Figure 42). The actual concentration enhances with increase in $x+\gamma t$ and reduces with higher $x+\gamma t = 2\pi$ (Figure 43).

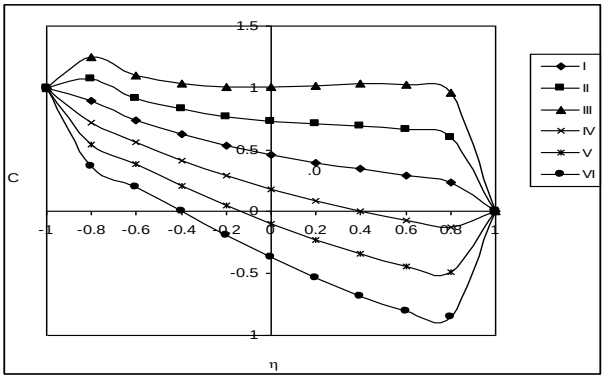

Fig. 33. Variation of C with G

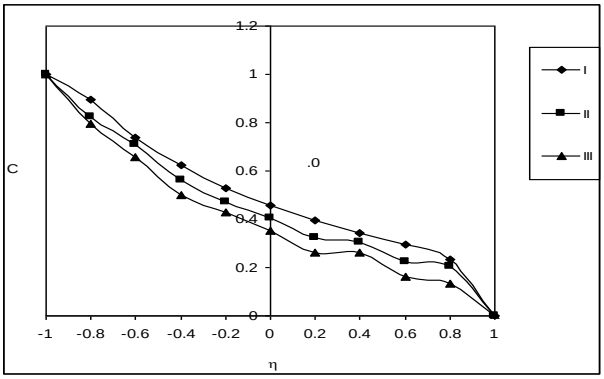

Fig. 34. Variation of C with R

	I	II	III	IV	V	VI
G	100	300	500	-100	-300	-500

	I	II	III
R	35	70	140

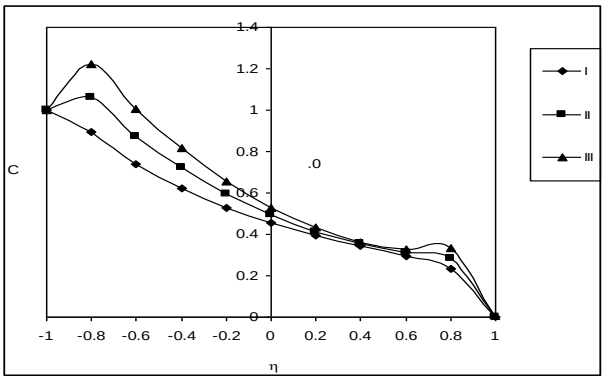

Fig. 35. Variation of C with M

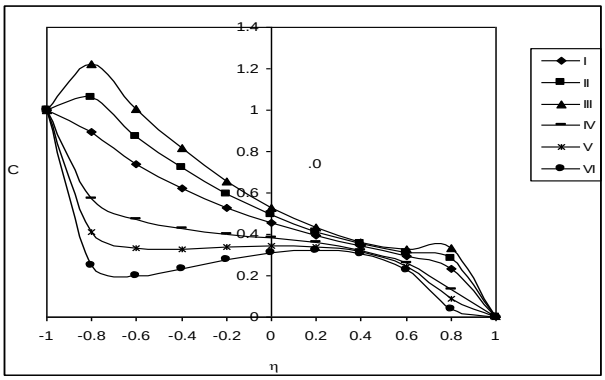

Fig. 36. Variation of C with α

	I	II	III
M	2	4	6

	I	II	III	IV	V	VI
α	2	4	6	-2	-4	-6

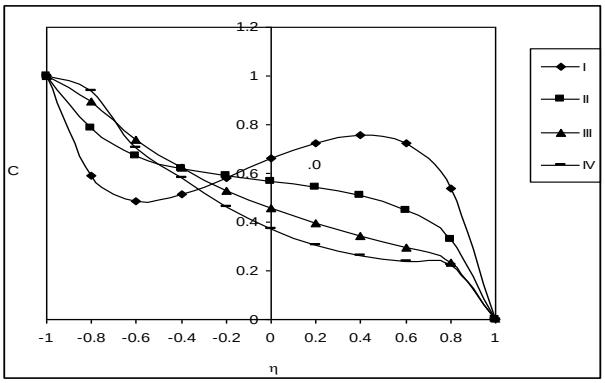

Fig. 37. Variation of C with Sc

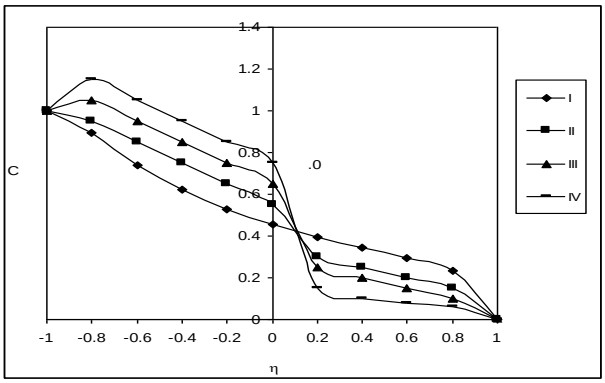

Fig. 38. Variation of C with Q_1

	I	II	III	IV
Sc	0.24	0.6	1.3	2.01

	I	II	III	IV
Q_1	0.5	1	1.5	2

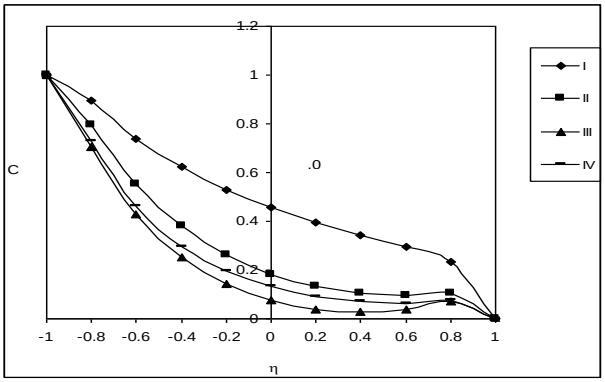

Fig. 39. Variation of C with k

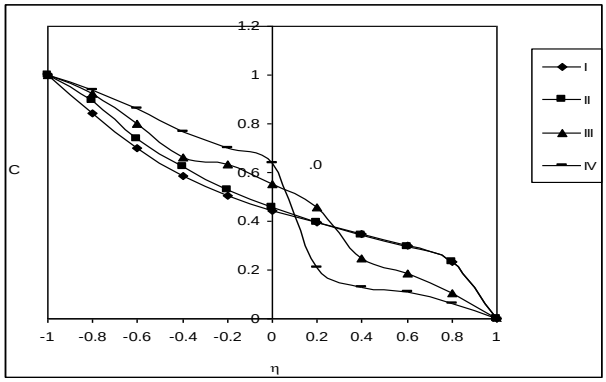

Fig. 40. Variation of C with β

	I	II	III	IV		I	II	III	IV
k	0.5	1.5	2.5	3.5	β	0.3	0.5	0.7	0.9

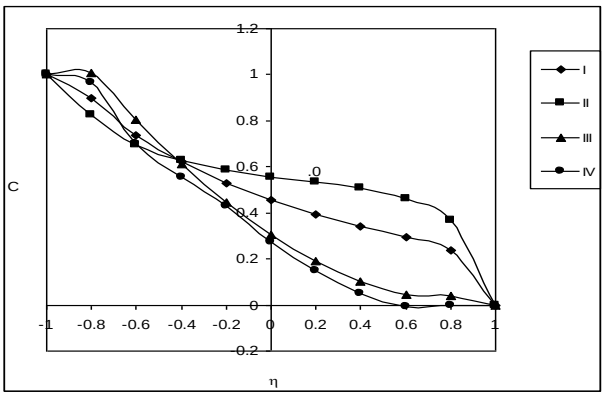

Fig. 41. Variation of C with N

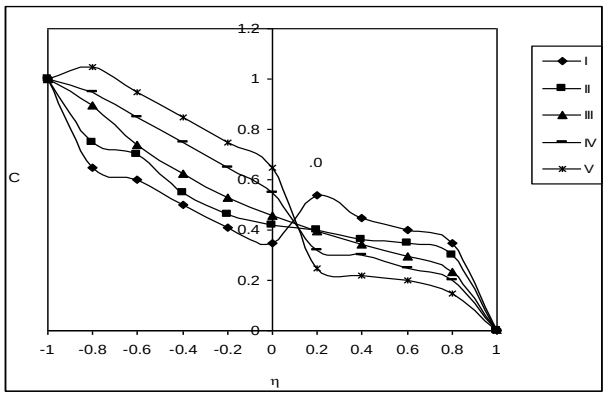

Fig. 42. Variation of C with E_c

	I	II	III	IV		I	II	III	IV	V
N	1	2	-0.5	-0.8	E_c	0.01	0.03	0.05	0.07	0.09

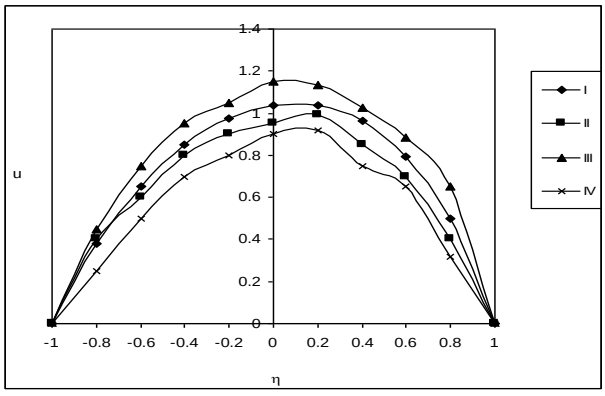

Fig. 43. Variation of C with x+γt

	I	II	III	IV
x+γt	π/4	π/2	π	2π

The local rate of heat transfer (Nusselt number) at η = ±1 is shown in Table 1 to Table 10 for different values of G, R, M, Sc, Q_1, N, k, β, Ec and x+γt. It is found that the rate of heat transfer enhances at η = ±1 with increase in G>0 and for G<0, |Nu| depreciates at η = +1 and enhances at η = -1 in the heating case while in the cooling case it reduces at η = +1 and enhances at η = -1. The variation of Nu with M shows that at η = +1, |Nu| enhances with M≤4 and for higher M≥6, it

enhances for G>0 and reduces for G<0. At $\eta = -1$, |Nu| reduces with M for all G. The variation of Nu with the phase $x+\gamma t$ of the boundary temperature shows that the rate of heat transfer enhances with smaller and higher values of $x+\gamma t$ in the heating case and reversed effect is observed in |Nu| in the cooling case at both the walls (Table 1and Table 6). The variation of Nu with heat source parameter α shows that at $\eta = +1$, |Nu| enhances for G>0 and reduces for G<0 with increase in the strength of the heat source and at $\eta = -1$, it reduces for all G, while for $\alpha<0$, it reduces in the heating case and enhances in the cooling case, at $\eta = \pm 1$, (tables 2&7). With respect to Schmidt number Sc, we find that lesser the molecular diffusivity larger |Nu| at $\eta = \pm 1$ in the heating case and in the cooling case |Nu| reduces at $\eta = +1$ and enhances at $\eta = -1$. An increase in the radiation absorption parameter Q_1 leads to a depreciation in |Nu| at $\eta = +1$ and an enhancement at $\eta = -1$. With respect to β it can be seen that the rate of heat transfer reduces |Nu| with $\beta \leq 0.5$ and enhances with higher $\beta \geq 0.7$ at both the walls (Tables 3 and Table 8). When the molecular buoyancy force dominates over the thermal buoyancy force |Nu| enhances at $\eta = \pm 1$ for G>0 and for G<0, it reduces at $\eta=+1$ and enhances at at $\eta = -1$ when the buoyancy forces act in the same direction and for the forces acting in opposite directions, |Nu| enhances at $\eta = +1$ and reduces at $\eta = -1$. The rate of heat transfer depreciates with increase in $k \leq 1.5$ and enhances with higher 1.5 at $\eta=\pm 1$ (Tables 4 and Table 9). From Table 5 and Table 10 we find that the rate of heat transfer enhances at $\eta=+1$ and reduces at $\eta = -1$ with increasing Ec in the heating case while in the cooling case it reduces at both the walls. Thus higher the dissipative heat larger |Nu| at $\eta = \pm 1$ and smaller at $\eta = -1$ for G>0 and for G<0, smaller (Nu| at $\eta = \pm 1$.

Table 1
Average Nusselt number (Nu) at y = +1

G	I	II	III	IV	V	VI	VII	VIII
10^3	0.0063	-0.2949	-0.3711	-1.8401	-1.9169	0.1186	-0.0932	-0.1889
$3x10^3$	-1.1844	-1.5453	7.6509	-1.7860	-1.9225	-1.2281	-1.0638	-1.1083
-10^3	-0.5110	-0.4929	-0.4773	-2.9093	-1.9389	-0.4823	-0.5901	-0.5609
$-3x10^3$	-0.5204	-0.5142	-0.5051	-1.9988	-1.9298	-0.4622	-0.5307	-0.5121
R	35	70	140	35	35	35	35	35
M	5	5	5	10	15	5	5	5
$x+\gamma t$	$\pi/4$	$\pi/4$	$\pi/4$	$\pi/4$	$\pi/4$	$\pi/2$	π	2π

Table 2
Average Nusselt number (Nu) at y = +1

G	I	II	III	IV	V	VI
10^3	0.0063	-0.5299	-0.7214	-0.9764	-0.8987	-0.8660
$3x10^3$	-0.4844	-0.7242	-0.8277	-0.9651	-0.9589	-0.9419
-10^3	-0.5110	-0.5829	-0.6220	0.1209	0.7548	-1.8676
$-3x10^3$	-0.4804	-0.5776	-0.6274	-0.0023	0.6270	2.4821
α	2	4	6	-2	-4	-6

Table 3
Average Nusselt number (Nu) at y = +1

G	I	II	III	IV	V	VI	VII	VIII	IX	X
10^3	0.0710	-0.3047	0.0163	-0.3421	0.0103	0.0095	0.0085	-10.4467	-0.2571	-0.3712
$3x10^3$	-0.1207	-0.4886	-1.1844	02.0792	-1.0844	-0.954	-0.9014	-0.8278	-0.3057	0.9089
-10^3	0.3018	-0.1655	-0.5110	-0.4921	-0.3610	-0.2524	-0.2095	-0.4410	-0.5477	-0.5650
$-3x10^3$	0.6254	0.1376	-0.4804	-0.4593	-0.4004	-0.3512	-0.3096	-0.3383	-0.5652	-0.6063
Sc	0.24	0.6	1.3	2.01	1.3	1.3	1.3	1.3	1.3	1.3
β	0.5	0.5	0.5	0.5	0.5	0.5	0.5	0.3	0.7	0.9

Table 4
Average Nusselt number (Nu) at y = +1

G	I	II	III	IV	V	VI	VII
10^3	-0.6063	-1.4592	-0.5158	-1.5468	-0.5418	-5.0873	34.6988
$3x10^3$	-1.1844	-1.2607	-0.4736	-1.6762	-0.7982	-11.9711	-49.6355
-10^3	-0.5110	-0.5016	0.1219	3.0234	-0.3033	5.7107	-17.5893
$-3x10^3$	-0.4804	-0.1748	-1.2012	-1.69774	-0.0788	27.5725	-37.9570
N	1	2	-0.5	-0.8	1	1	1
k	0.5	0.5	0.5	0.5	1.5	2.5	3.5

Table 5
Average Nusselt number (Nu) at y = +1

G	I	II	III	IV	V
10^3	-0.0111	-0.0284	0.0363	0.0434	0.0830
$3x10^3$	-1.1175	-1.1554	-1.1844	-1.2073	-1.2259
-10^3	-0.5366	-0.5239	-0.5110	-0.4978	-0.4843
$-3x10^3$	-0.5914	-0.5387	-0.4804	-0.4158	-0.3436
Ec	0.01	0.03	0.05	0.07	0.09

Table 6
Average Nusselt number (Nu) at y = -1

G	I	II	III	IV	V	VI	VII	VIII
10^3	2.0486	2.4859	3.1064	-0.1285	-0.0606	3.1417	1.8105	8.1274
$3x10^3$	-5.3604	-9.8826	-14.3051	-0.1423	-0.0802	-3.6521	-2.7540	-12.9506
-10^3	-0.8566	-0.9495	-1.0090	0.2316	0.1106	-0.8073	-1.0300	-0.9584
$-3x10^3$	-1.6057	-1.8189	-2.0086	0.3496	0.2602	-1.5467	-1.7944	-1.7198
R	35	70	140	35	35	35	35	35
M	5	5	5	10	15	5	5	5
$x+\gamma t$	$\pi/4$	$\pi/4$	$\pi/4$	$\pi/4$	$\pi/4$	$\pi/2$	π	2π

Table 7
Average Nusselt number (Nu) at y = -1

G	I	II	III	IV	V	VI
10^3	4.0486	0.6363	0.1503	-1.3812	-1.0425	-0.8871
$3x10^3$	-3.3604	1.8832	0.5294	-1.4483	-1.2847	-1.1618
-10^3	-0.8566	-0.4023	-0.1326	-4.9654	60.7819	7.0139
$-3x10^3$	-1.6057	-0.9226	-0.3599	-3.9729	-6.7404	-14.9052
α	2	4	6	-2	-4	-6

Table 8
Average Nusselt number (Nu) at y = -1

G	I	II	III	IV	V	VI	VII	VIII	IX	X
10^3	-0.0141	-0.2982	-1.6486	2.0810	1.8486	2.9292	2.1296	-1.3863	1.9480	2.1286
$3x10^3$	-0.0125	-0.2361	-3.3604	5.8921	-3.4609	-3.8619	-3.9526	-1.2855	-3.4592	-3.2482
-10^3	-0.0158	-0.2601	-0.8566	-0.7835	-0.9066	-0.9526	-0.9896	-0.5982	-0.9091	-1.0125
$-3x10^3$	-0.0185	-0.3375	-1.6057	-1.9198	-1.6267	-1.8596	-1.9256	-0.9958	-1.9509	-2.0126
Sc	0.24	0.6	1.3	2.01	1.3	1.3	1.3	1.3	1.3	1.3
β	0.5	0.5	0.5	0.5	0.5	0.5	0.5	0.3	0.7	0.9

Table 9
Average Nusselt number (Nu) at y = -1

G	I	II	III	IV	V	VI	VII
10^3	4.0486	-4.6452	-0.8844	0.4889	0.1323	0.1511	-0.3730
$3x10^3$	-4.3604	-4.8172	-1.6378	0.1757	0.4018	0.3690	1.9824
-10^3	-0.8566	-1.4151	2.8777	1.9842	-0.1315	-0.2031	0.6629
$-3x10^3$	-1.6057	-2.6908	-3.1737	-2.4223	-0.3942	-0.9847	0.3386
N	1	2	-0.5	-0.8	1	1	1
K	0.5	0.5	0.5	0.5	1.5	2.5	3.5

Table 10
Average Nusselt number (Nu) at y = -1

G	I	II	III	IV	V
10^3	4.2833	4.1705	4.0846	3.9162	3.7721
$3x10^3$	-4.9009	-4.0377	-3.3604	-2.8147	-2.3657
-10^3	-0.9609	-0.9093	-0.8566	-0.8029	-0.7841
$-3x10^3$	-1.6578	-1.6331	-1.6057	-1.5752	-1.5409
Ec	0.01	0.03	0.05	0.07	0.09

The rate of mass transfer (Sherwood number) at $\eta = \pm 1$ is exhibited in Tables 11 to Table 20 for different parametric values. It is found that the rate of mass transfer enhances at $\eta = +1$ and depreciates at $\eta = -1$ with increase in G>0 and for G< 0 |Sh| enhances at both the walls. An increase in R reduces |Sh| at $\eta = +1$ and enhances at $\eta = -1$ in the heating case while in the cooling case, it depreciates at $\eta = \pm 1$. With respect M we find that higher the Lorentz force larger |Sh| at both the walls. An increase in the phase $x+\gamma t \leq \pi$, enhances |Sh| at $\eta = +1$ and reduces at $\eta = -1$, while for higher $x+\gamma t \geq 2\pi$, it reduces at $\eta = +1$ and enhances at $\eta = -1$ (Table 11 and Table 16). The variation of Sh with heat source parameter α shows that |Sh| reduces with $\alpha>0$ and enhances with $\alpha<0$ at $\eta = +1$ while at $\eta = -1$, it enhances with $\alpha>$Sh| at $\eta = +1$ and enhances at $\eta = -1$ and for higher $Q_1 \geq 2$, it enhances at $\eta = +1$ and reduces at $\eta = -1$ (Table 13 and Table 18). When the molecular buoyancy force dominates over the thermal buoyancy force the rate of mass transfer enhances at $\eta = \pm 1$ when the buoyancy forces act in the same direction and for the forces acting in opposite directions |Sh| enhances at $\eta = +1$and depreciates at $\eta = -1$. The variation of Sh with chemical reaction parameter k shows that |Sh|| at $\eta = +1$ depreciates with $k \leq 1.5$ and enhances with higher $|k| \geq 2.5$ and at $\eta = -1$, |Sh| enhances with k for all G. An increase in $Ec \leq 0.01$ enhances |Sh| for G>0 and reduces for G<0 and for higher $Ec \geq 0.09$, it enhances for all G. At $\eta = -1$, |Sh| enhances with $Ec \leq 0.07$ and reduces with higher $Ec \geq 0.09$ (Table 15 and Table 20).

Table 11
Average Sherwood Number (Sh) at y = +1

G	I	II	III	IV	V	VI	VII	VIII
10^3	0.0758	0.0756	0.0755	0.3983	5.0483	0.0984	0.1654	0.1242
$3x10^3$	0.2145	0.2139	0.2137	1.3284	-6.4322	0.2586	0.3652	0.3242
-10^3	-0.0579	-0.0575	-0.0572	-0.3417	-2.0787	-0.0786	-0.0846	-0.8042
$-3x10^3$	-0.1868	-0.1864	-0.1862	-0.9445	-3.9396	-0.2842	-0.3126	-0.2942
R	35	70	140	35	35	35	35	35
M	5	5	5	10	15	5	5	5
$x+\gamma t$	$\pi/4$	$\pi/4$	$\pi/4$	$\pi/4$	$\pi/4$	$\pi/2$	π	2π

Table 12
Average Sherwood Number (Sh) at y = +1

G	I	II	III	IV	V	VI
10^3	0.0758	0.0506	0.0257	0.1272	0.1534	0.1800
$3x10^3$	0.2145	0.1358	0.0601	0.3818	0.4707	0.5635
-10^3	-0.0579	-0.0337	-0.0092	-0.1054	-0.1287	-0.1517
$-3x10^3$	-0.1868	-0.1171	-0.0446	-0.3188	-0.3812	-0.4414
α	2	4	6	-2	-4	-6

Table 13
Average Sherwood Number (Sh) at y = +1

G	I	II	III	IV	V	VI	VII	VIII	IX	X
10^3	0.0131	0.0380	0.0758	0.0963	0.0658	0.0549	0.0849	0.0676	0.0873	0.1026
$3x10^3$	0.0351	0.1041	0.2145	0.2798	0.2046	0.1948	0.2296	0.1887	0.2521	0.3043
-10^3	-0.0090	-0.0274	-0.0579	-0.0761	-0.0526	-0.0506	-0.0626	-0.0515	-0.0675	-0.0806
$-3x10^3$	-0.0309	-0.0922	-0.1868	-0.2383	-0.1762	-0.1729	-0.1969	-0.1685	-0.2130	-0.2475
Sc	0.24	0.6	1.3	2.01	1.3	1.3	1.3	1.3	1.3	1.3
β	0.5	0.5	0.5	0.5	0.5	0.5	0.5	0.3	0.7	0.9

Table 14
Average Sherwood Number (Sh) at y = +1

G	I	II	III	IV	V	VI	VII
10^3	0.0758	0.1708	-0.0611	0.1507	0.0436	0.0996	-0.3284
$3x10^3$	0.2145	0.5216	-0.1944	0.4382	0.1211	0.3110	-0.8978
-10^3	-0.0579	-0.1462	0.0798	0.1082	-0.0312	-0.0893	0.3671
$-3x10^3$	-0.1868	-0.4340	0.2292	0.3198	-0.1034	-0.2592	1.2357
N	1	2	-0.5	-0.8	1	1	1
K	0.5	0.5	0.5	0.5	1.5	2.5	3.5

Table 15
Average Sherwood Number (Sh) at y = +1

G	I	II	III	IV	V
10^3	0.0558	0.0628	0.0758	0.0849	0.0950
$3x10^3$	0.1945	0.2042	0.2145	0.2249	0.2353
-10^3	-0.0779	-0.0628	-0.0579	-0.0684	-0.0786
$-3x10^3$	-0.2069	-0.1949	-0.1868	-0.1984	-0.2164
Ec	0.01	0.03	0.05	0.07	0.09

Table 16
Average Sherwood Number (Sh) at y = -1

G	I	II	III	IV	V	VI	VII	VIII
10^3	0.0523	0.0533	0.0538	-0.0843	-2.3627	0.516	0.0496	0.0564
$3x10^3$	0.0162	0.0192	0.0208	-0.4579	11.8070	0.0152	0.0149	0.0164
-10^3	0.0870	0.0861	0.0856	0.2071	0.9977	0.0742	0.0712	0.0745
$-3x10^3$	0.1204	0.1176	0.1161	0.4407	1.7896	0.1182	0.1169	0.1284
R	35	70	140	35	35	35	35	35
M	5	5	5	10	15	5	5	5
$x+\gamma t$	$\pi/4$	$\pi/4$	$\pi/4$	$\pi/4$	$\pi/4$	$\pi/2$	π	2π

Table 17
Average Sherwood Number (Sh) at y = -1

G	I	II	III	IV	V	VI
10^3	0.0523	0.0592	0.0661	0.0382	0.0310	0.0236
$3x10^3$	0.0162	0.0378	0.0586	-0.0300	-0.0267	-0.0206
-10^3	0.0870	0.0804	0.0737	0.1001	0.1064	0.1127
$-3x10^3$	0.1204	0.1013	0.0814	0.1564	0.1733	0.1897
α	2	4	6	-2	-4	-6

Table 18
Average Sherwood Number (Sh) at y = -1

G	I	II	III	IV	V	VI	VII	VIII	IX	X
10^3	0.0111	0.0299	0.0523	0.0704	0.0623	0.0645	0.0512	0.0733	0.0695	-0.0989
$3x10^3$	0.0236	0.0472	0.0662	0.0802	0.186	0.189	0.164	0.1136	-0.1272	-0.3332
-10^3	-0.0012	0.0127	0.0870	0.1917	0.0912	0.1984	0.0842	0.0338	0.1562	0.2433
$-3x10^3$	-0.136	-0.0143	0.1204	0.3045	0.1245	0.1286	0.1246	-0.0154	0.2838	0.488
Sc	0.24	0.6	1.3	2.01	1.3	1.3	1.3	1.3	1.3	1.3
β	0.5	0.5	0.5	0.5	0.5	0.5	0.5	0.3	0.7	0.9

Table 19
Average Sherwood Number (Sh) at y = -1

G	I	II	III	IV	V	VI	VII
10^3	0.0523	0.0272	0.0884	0.0293	0.2569	0.3303	1.5214
$3x10^3$	0.0162	0.0655	0.1239	0.04804	0.1150	-1.0289	2.4302
-10^3	0.0870	0.1102	0.0507	0.0432	0.3910	1.0064	-1.1389
$-3x10^3$	0.1204	0.1851	0.0106	0.0095	0.5180	1.6918	-4.1399
N	1	2	-0.5	-0.8	1	1	1
K	0.5	0.5	0.5	0.5	1.5	2.5	3.5

Table 20
Average Sherwood Number (Sh) at y = -1

G	I	II	III	IV	V
10^3	0.0513	0.1543	0.1642	0.1710	0.1589
$3x10^3$	0.0152	0.0156	0.0165	0.0174	0.0164
-10^3	0.0862	0.0874	0.0912	0.1002	0.0954
$-3x10^3$	0.1164	0.1189	0.1212	0.1224	0.1106
Ec	0.01	0.03	0.05	0.07	0.09

8. Conclusion

In this paper, we considered the unsteady thermal convection due to the imposed traveling thermal wave boundary through a vertical channel bounded by flat walls. The computed results can be summarized as follow

- An increase in the Reynolds number R depreciates with increase in R.
- An increase in the radiation absorption Q_1 results in an enhancement in $|u|.\backslash$
- The variation of C with Ec shows that higher the dissipative heat larger the actual concentration in the left half and smaller in the right half of the channel.
- The actual concentration enhances with increase in $x+\gamma t$ and reduces with higher $x+\gamma t = 2\pi$.
- The rate of heat transfer depreciates with increase in $k \leq 1.5$ and enhances with higher 1.5 at $\eta = \pm 1$
- we find that the rate of heat transfer enhances at $\eta = +1$ and reduces at $\eta = -1$ with increasing Ec in the heating case while in the cooling case it reduces at both the walls.

Acknowledgment

The author would also like to acknowledge Manipal academy of Higher Education support for this study.

References

[1] Somers, E. V. "Theoretical considerations of combined thermal and mass transfer from a vertical flat plate." *J. Appl. Mech* 23, no. 29 (1956): 301.
[2] Gill, William N., Eduardo Del Casal, and Dale W. Zeh. "Binary diffusion and heat transfer in laminar free convection boundary layers on a vertical plate." *International Journal of Heat and Mass Transfer* 8, no. 8 (1965): 1135-1151.
[3] Adams, James A., and Robert L. Lowell Jr. "Free convection organic sublimation on a vertical semi-infinite plate." *International Journal of Heat and Mass Transfer* 11, no. 8 (1968): 1215-1224.
[4] Gebhart, B., and L. Pera. "Natural convection flows adjacent to horizontal surface resulting from the combined buoyancy effects of thermal diffusion." *Int. J. Heat Mass Transf* 15 (1971): 269-278.
[5] Lavanya, B. "Unsteady MHD Convective laminar flow between two Vertical Porous plates with mass transfer." *Journal of Mechanical Engineering Research and Developments* 47 (2018): 97-109.
[6] Nelson, Douglas J., and B. D. Wood. "Combined heat and mass transfer natural convection between vertical parallel plates." *International Journal of Heat and Mass Transfer* 32, no. 9 (1989): 1779-1787.
[7] Nelson D.J. and Wood B.D *: J. Heat transfer V.4, PP-1587-1582(1986).*
[8] Nagasasikala, Madduleti, and Bommanna Lavanya. "Effects of Dissipation and Radiation on Heat Transfer Flow of a Convective Rotating Cuo-Water Nano-fluid in a Vertical Channel." *Journal of Advanced Research in Fluid Mechanics and Thermal Sciences* 50, no. 2 (2018): 108-117.
[9] Lavanya, Bommanna. "MHD Rotating Flow Through a Porous Medium with Heat and Mass Transfer." *Journal of Advanced Research in Fluid Mechanics and Thermal Sciences* 54, no. 2 (2019): 221-231.
[10] Vajravelu, K., and L. Debnath. "Nonlinear study of convective heat transfer and fluid flows induced by travelling thermal waves." *Acta mechanica* 59, no. 3-4 (1986): 233-249.
[11] Lavanya B et.al. "Radiation and chemical reaction effects on MHD flow over an infinite vertical oscillating porous plate with soret effect." *International Journal of Mathematical Archive EISSN* 4, no. 9 (2013): 2229-5046.
[12] Lavanya, B et al. "Radiation and mass transfer effects on MHD Marangoni convection over a flat surface in presence of joule heating Viscous dissipation heat generation with suction and injection." *i-Manager's Journal on Mathematics* 3, no. 3 (2014): 34.
[13] Guria, M., and R. N. Jana. "Hydrodynamic flows through vertical wavy channel with travelling thermal waves embedded in porous medium." *APPLIED MECHANICS AND ENGINEERING* 11, no. 3 (2006): 609.
[14] G. Y. Ny, N. H. Barom, S. M. Noraziman and S. T. Yeow. "Numerical Study on Turbulent-Forced Convective Heat Transfer of Ag/Heg Water Nanofluid in Pipe." *Journal of Advanced Research in Materials Science* 22 (2016): 11 – 27.
[15] Dero, Sumera, Azizah Mohd Rohni, and Azizan Saaban. "MHD micropolar nanofluid flow over an exponentially stretching/shrinking surface: Triple solutions." *J. Adv. Res. Fluid Mech. Therm. Sci* 56, no. 2 (2019): 165-174.
[16] H.A. Mohammed, O. A. Alawi, N. A. Che Sidik. "Mixed Convective Nanofluids Flow in a Channel having Forward-Facing Step with Baffle Page." *Journal of Advanced Research in Applied Mechanics* 24 (2016): 1 – 21.
[17] Lavanya, B. "Effect of radiation on free convection heat and mass transfer flow through porous medium in a vertical channel with heat absorption/generation and chemical reaction." In *AIP Conference Proceedings*, vol. 1859, no. 1, p. 020023. AIP Publishing, 2017.